

**LASER SPECTROSCOPY OF STIMULATED
SCATTERING IN COLLISIONALLY BROADENED
GROUP IIA METAL VAPORS**

Jim Kelly

Department of Physics
University of Idaho
Moscow, ID 83843

DTIC
ELECTE
JAN 5 1993
S C D

November 1992

Final Report

**APPROVED FOR PUBLIC RELEASE; DISTRIBUTION IS
UNLIMITED.**

93-00197



**PHILLIPS LABORATORY
Lasers and Imaging Directorate
AIR FORCE MATERIEL COMMAND
KIRTLAND AIR FORCE BASE, NM 87117-6008**

This final report was prepared by the University of Idaho, Moscow, Idaho, under contract F29601-88-C-0024, Job Order 33261B20, with the Phillips Laboratory, Kirtland Air Force Base, New Mexico. The Phillips Laboratory Project Officer-in-Charge was Dr. Christopher M. Clayton (LIT).

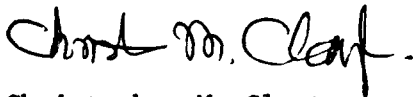
When Government drawings, specifications, or other data are used for any purpose other than in connection with a definitely Government-related procurement, the United States Government incurs no responsibility or any obligation whatsoever. The fact that the Government may have formulated or in any way supplied the said drawings, specifications, or other data, is not to be regarded by implication, or otherwise in any manner construed, as licensing the holder, or any other person or corporation; or as conveying any rights or permission to manufacture, use, or sell any patented invention that may in any way be related thereto.

This report has been authored by a contractor of the United States Government. Accordingly, the United States Government retains a nonexclusive royalty-free license to publish or reproduce the material contained herein, or allow others to do so, for the United States Government purposes.

This report has been reviewed by the Public Affairs Office and is releasable to the National Technical Information Service (NTIS). At NTIS, it will be available to the general public, including foreign nationals.

If your address has changed, if you wish to be removed from our mailing list, or if your organization no longer employs the addressee, please notify PL/LIT to help us maintain a current mailing list.

This report has been reviewed and is approved for publication.

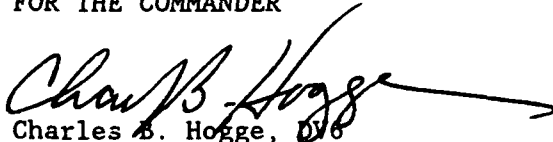


Christopher M. Clayton
Project Officer



Bruce A. Conway, Lt Col USAF
Chief, Technology Division

FOR THE COMMANDER



Charles B. Hogge, DVO
Acting Director
Lasers and Imaging Directorate

DO NOT RETURN COPIES OF THIS REPORT UNLESS CONTRACTUAL OBLIGATIONS OR NOTICE ON A SPECIFIC DOCUMENT REQUIRES THAT IT BE RETURNED.

REPORT DOCUMENTATION PAGE

Form Approved
OMB No. 0704-0188

Public reporting burden for this collection of information is estimated to average 1 hour per response, including the time for reviewing instructions, searching existing data sources, gathering and maintaining the data needed, and completing and reviewing the collection of information. Send comments regarding this burden estimate or any other aspect of this collection of information, including suggestions for reducing this burden, to Washington Headquarters Services, Directorate for Information Operations and Reports, 1215 Jefferson Davis Highway, Suite 1204, Arlington, VA 22202-4302, and to the Office of Management and Budget, Paperwork Reduction Project (0704-0188), Washington, DC 20503.

1. AGENCY USE ONLY (Leave blank)	2. REPORT DATE November 1992	3. REPORT TYPE AND DATES COVERED Final Report 1 Oct 88 - 1 Apr 92
----------------------------------	---------------------------------	--

4. TITLE AND SUBTITLE LASER SPECTROSCOPY OF STIMULATED SCATTERING IN COLLISIONALLY BROADENED GROUP IIA METAL VAPORS	5. FUNDING NUMBERS C: F29601-88-C-0024 PE: 65502F PR: 3326 TA: 1B WU: 20
---	---

6. AUTHOR(S) Jim Kelly	
-------------------------------	--

7. PERFORMING ORGANIZATION NAME(S) AND ADDRESS(ES) Department of Physics University of Idaho Moscow, ID 83843	8. PERFORMING ORGANIZATION REPORT NUMBER
--	---

9. SPONSORING / MONITORING AGENCY NAME(S) AND ADDRESS(ES) Phillips Laboratory Kirtland AFB, NM 87117-6008	10. SPONSORING / MONITORING AGENCY REPORT NUMBER PL TR-92-1040
---	--

11. SUPPLEMENTARY NOTES

12a. DISTRIBUTION / AVAILABILITY STATEMENT Approved for public release; distribution is unlimited.	12b. DISTRIBUTION CODE
---	------------------------

13. ABSTRACT (Maximum 200 words)

This study is concerned with the development of efficient nonlinear materials which can generate 3-5 μ m infrared (IR). Work involved the use of Ca and Sr metal vapors as electronic Raman scattering (SRS). This involved the development of narrow bandwidth pulse lasers, scattering cells, high speed IR detectors, and suitable experimental diagnostics to study the gain for SRS and its temporal development. It was found that SRS was never generated, but instead, a variety of other nonlinear responses were readily induced, the most notable being superfluorescence (SF). Results of these studies of SF in the optically trapped principal resonance state of Ca(Sr) may be useful in the development or diagnostics of plasma based x-ray lasers.

14. SUBJECT TERMS nonlinear optics, metal vapors, stimulated scattering, laser spectroscopy	15. NUMBER OF PAGES 58
	16. PRICE CODE

17. SECURITY CLASSIFICATION OF REPORT Unclassified	18. SECURITY CLASSIFICATION OF THIS PAGE Unclassified	19. SECURITY CLASSIFICATION OF ABSTRACT Unclassified	20. LIMITATION OF ABSTRACT SAR
--	---	--	---------------------------------------

PREFACE

This report details studies of the nonlinear gain to produce stimulated Raman scattering in the Group IIA metal vapors of Ca and Sr. The results were performed by Dr. Jim Kelly in conjunction with a PhD candidate A. Kumarakrishnan and postdoctoral associate Dr Xianming Han, under the auspices of the Physics Department at the University of Idaho. The Air Force program manager was Dr Chris Clayton, Nonlinear Optics Center of Technology, Phillips Laboratory, Kirtland AFB, New Mexico.

DECLASSIFIED

Accession For	
NTIS Grant	<input checked="checked" type="checkbox"/>
D749 TAB	<input type="checkbox"/>
Unannounced	<input type="checkbox"/>
Justification	
By	
Distribution/	
Availability Codes	
Dist	Avail and/or Special
A-1	

CONTENTS

<u>Section</u>		<u>Page</u>
1.0	INTRODUCTION	1
2.0	EXPERIMENTAL ARRANGEMENT	5
3.0	SPECTROSCOPY OF Ca AND Sr VAPOR	12
4.0	ELECTRONIC EXCITATION AND RELAXATION OF Ca(4^1P_1) AND Sr(5^1P_1)	16
4.1	SUPERFLUORESCENCE FROM Ca(4^1P_1)	16
4.2	COLLISION-INDUCED SF BY SPIN-CHANGING COLLISIONS WITH RARE GASES	27
4.3	MODIFICATION OF SF POLARIZATION BY COLLISIONAL REDISTRIBUTION OF RADIATION IN STRONG FIELDS	30
4.4	HYPER-RAMAN SCATTERING AND CASCADE SF EMISSIONS IN Ca	39
5.0	CONCLUSIONS	45
	REFERENCES	46

FIGURES

<u>Figure</u>		<u>Page</u>
1.	Primary electronic Raman levels involved in SRS in Ca and Sr.	2
2.	Temporal characteristics of SF.	3
3.	Experimental layout used in stimulated scattering experiments.	6
4.	An A-B comparison of IR detector and fast photodiode to 1.064 μm radiation.	8
5.	Partial term diagrams for Ca pump and probe scheme.	11
6.	Dressed states of Ca($4\ ^1\text{S}_0$ - $4\ ^1\text{P}_1$) transition in the presence of a strong laser field.	14
7.	Comparison of ground state [Ca($^1\text{S}_0$)] by the technique of equivalent width with saturated vapor pressure curve.	17
8.	Representative SF pulses at 5.5 μm .	19
9.	Comparison of forward and backward scattered SF emission pulse shapes.	20
10.	Comparison of SF evolution time $(\tau_{\text{R}}\tau_{\text{D}})^{\frac{1}{2}}$ with T_2^* as a function of the number of SF radiators N.	22
11.	Model calculations of SF-single shot realizations.	24
12.	Model calculation of SF for different rates of radiative redistribution.	25
13.	The SF emissions of the Ca($3\ ^3\text{D}_3$ - $4\ ^3\text{P}_2$) transition.	29
14.	Collisional redistribution pathways for the dressed levels of a $^1\text{S}_0$ - $^1\text{P}_1$ transition.	31
15.	Orientation of SF ellipticity of polarization versus laser detuning.	33
16.	Analysis of SF ellipticity orientation.	35
17.	Analysis of SF ellipticity orientation versus laser detuning.	36

FIGURES (Concluded)

<u>Figure</u>		<u>Page</u>
18.	Ratio of linear polarization components versus laser detuning.	38
19.	Two-photon and two-step collisionally aided excitation of Rydberg levels.	40
20.	Comparison of IR SF cascade and its successive optical SF emission.	44

1.0 INTRODUCTION

This report describes experimental studies of the stimulated scattering which is induced in the Group IIA metal vapors Ca and Sr when their principal resonance transition is optically pumped (Fig. 1). The primary impetus of this work was to study a longstanding issue of competition between stimulated Raman scattering (SRS) and alternate relaxation processes which inhibit SRS. The goal was to understand how to optimize the gain for SRS, thus producing tunable mid-IR emissions near 5.5 and 6.5 μm . An essential result of this work is that SRS is not readily produced in these vapors. Instead, a variety of nonlinear scattering and collisional redistribution processes occur which lead to strong superfluorescence (SF) emissions.

Superfluorescence is a cooperative emission process similar to Dicke superradiance (Ref. 1), except that the sample of N excited radiators is initially incoherent (Ref. 2). Coherence in a macroscopic sample with dimensions $d \gg \lambda_{\text{SF}}$ has been shown to develop from the random spontaneous emissions of the sample (Ref. 3). The SF is thus characterized by a finite time delay before the onset of cooperative emission. Under ideal conditions, the sample will rapidly develop a macroscopic polarization, thus emitting a strong brief pulse with peak height $\propto (N')^2$ and pulse width $\propto 1/N'$ where N' is the number of radiators that can participate in the collective emission. Figure 2 shows schematically the basic temporal features which exemplify SF emission. An unexpected discovery of this experimental investigation is the measurement of large quantum yields of IR emission by optically trapped $\text{Ca}(4^1\text{P}_1)$ even in the presence of fast radiative redistribution. The nature of the SF polarization was also investigated and was found to change abruptly due to collisional redistribution. The collisional transfer of population was found to be dependent on the intense light field of the pump laser, consistent with earlier studies (Refs. 4-6).

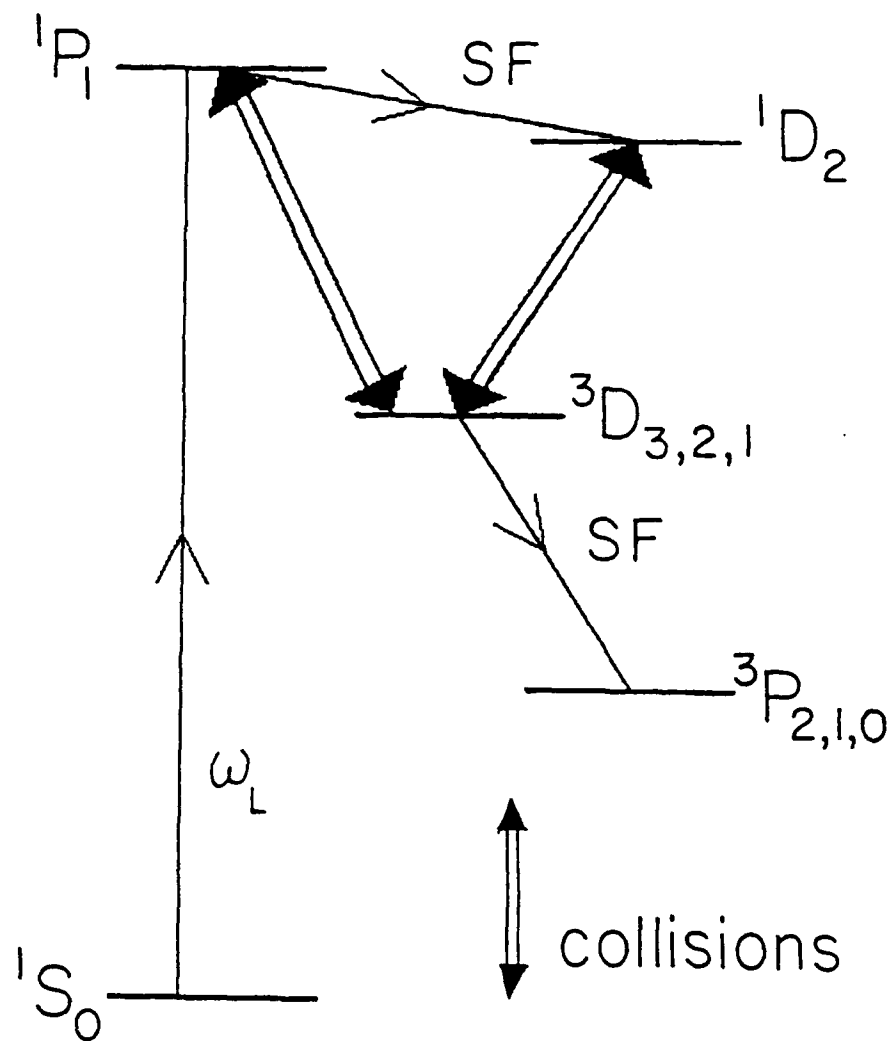


Figure 1. Primary electronic Raman levels involved in SRS in Ca and Sr.

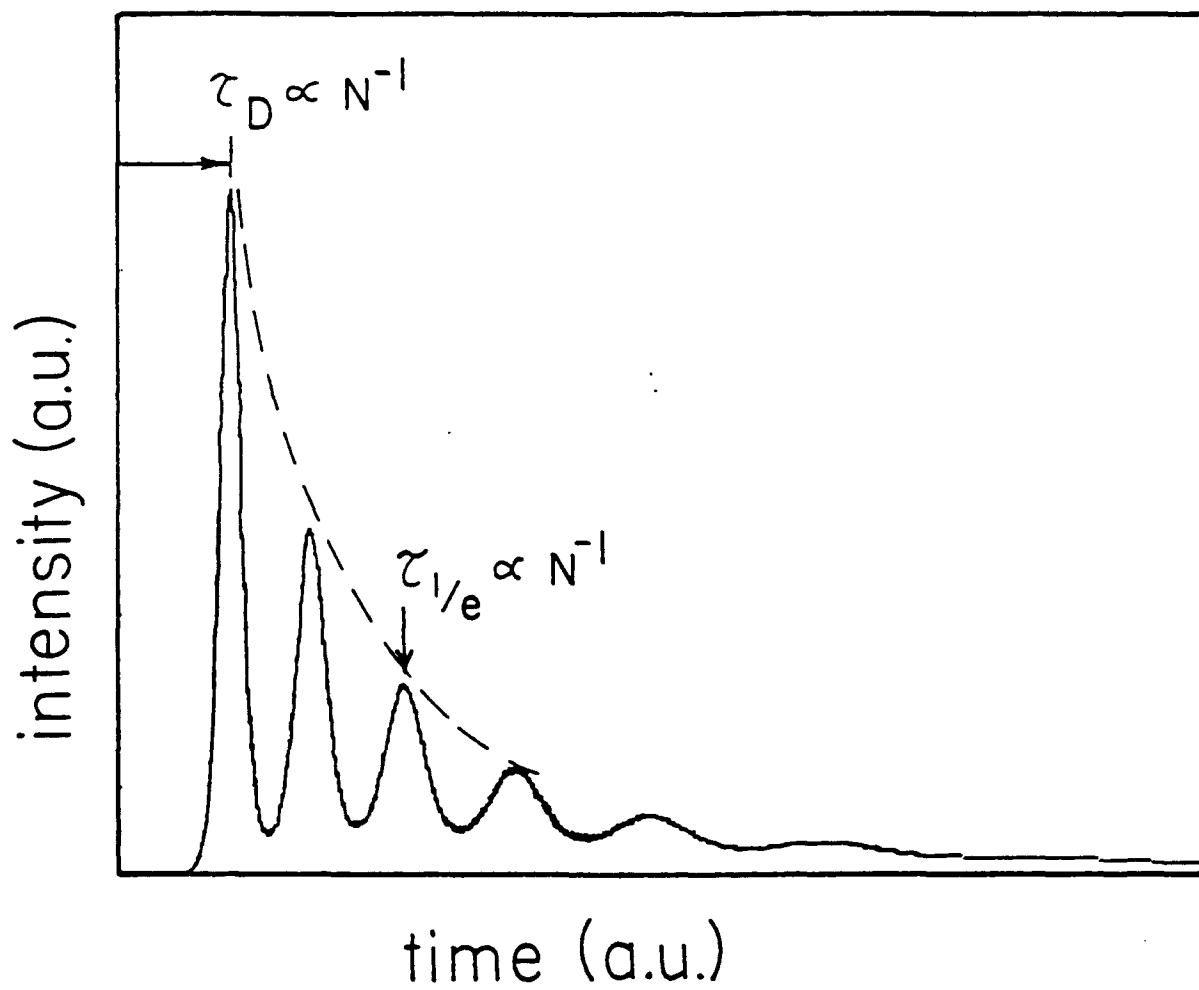


Figure 2. Temporal characteristics of SF.

Lastly, two-photon and two-step collisionally aided transfers were observed to high lying Rydberg states which resulted in visible and IR emissions by cascade SF emission. Many of the visible emissions were compressed substantially, resulting in 1-ns pulses which were the bandwidth limit of the apparatus.

2.0 EXPERIMENTAL ARRANGEMENT

A general schematic layout of the experimental arrangement is shown in Figure 3. The scattering experiments were performed in long uniform columns of metal vapors contained in two types of stainless steel cells of different designs. The first type used hot sapphire windows sealed to inner flanges by Helicoflex metal seals.* It was discovered that Ca vapor can readily diffuse into the sapphire despite operating the windows as much as 125°C above the ambient vapor temperature of the main section of the cell. The transmission properties of the sapphire degraded quickly (1-2 hr) to the point where the transmission of the pump laser (operated near 423 nm) was attenuated to <20 percent of the incident intensity. The Sr vapor is less reactive and permits >70-percent transmission after diffusing into the sapphire. This type of cell was abandoned subsequently in the Ca experiments for a second system which used knife edge baffles and small charges of Ar buffer gas to constrain the effusion of Ca from reaching the cold outer CaF₂ (or BaF₂) windows of the vacuum system. Water coils located between the heated baffles and CaF₂ windows were used to chill the Ar buffer gas, thus producing strong convective currents in the region just beyond the baffles. The path length of hot Ca vapor was well established by this technique, as evidenced by Ca deposits which built up immediately outside the knife edge baffles. This second cell had a path length of ~50 cm of active Ca vapor. It should be noted that measurements of SF in Ca were obtained with both type cells.

The column of Ca was excited by pulses from a multimode (1-2 GHz) dye laser system tuned in the vicinity of the $4s^2\ ^1S_0 - 4s4p\ ^1P_1$ principal resonance line near 423 nm. The dye laser consisted of a double-grating, grazing incidence oscillator and two or three stages of amplifiers. The spectral content of the amplified dye

* Helicoflex part types HNV200 and HN100-1 which consist of a nickel sheath drawn over an Inconel spring. Nickel seals are recommended for work with the Group IIA elements.

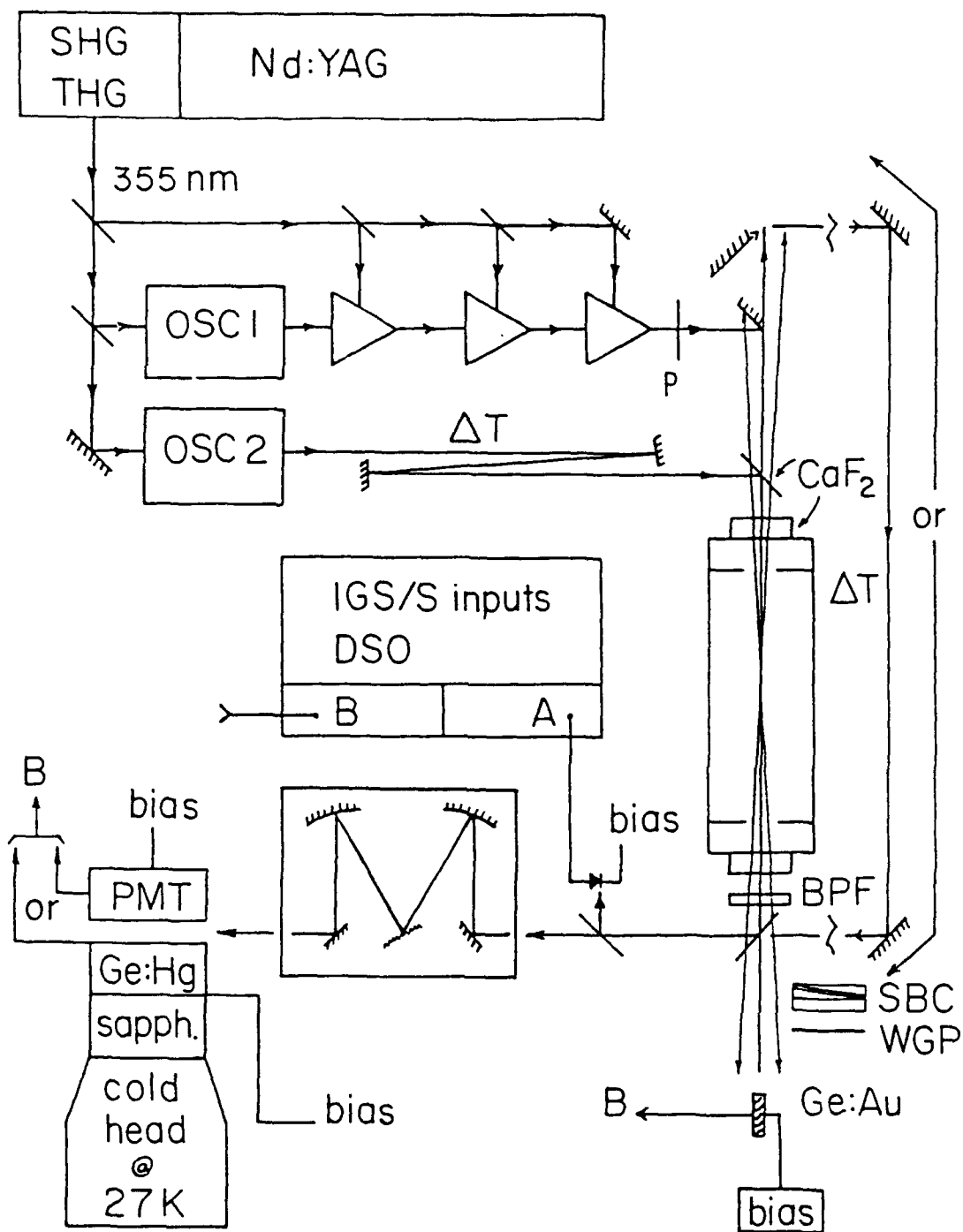
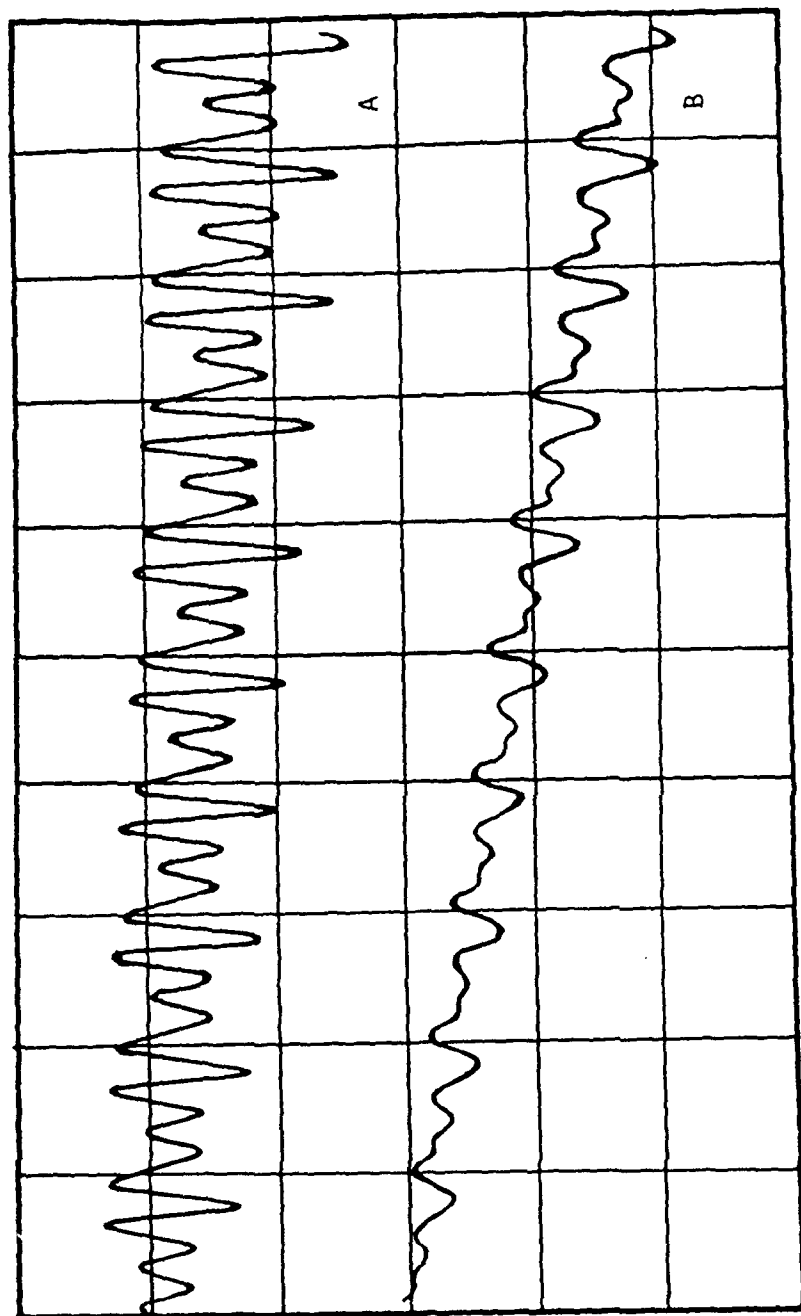


Figure 3. Experimental layout used in stimulated scattering experiments. P designates polarizer; SBC - Soleil-Babinet Compensator; WGP - Wire Grid Polarizer; BPF - Bandpass Filter; Ge: - Germanium Doped Photoconductors.

laser was studied with a 0.75-m double monochromator (Spex 1401). The measured ratio of total laser light to the broad amplified spontaneous emission (ASE) pedestal was $>6:1$ with the ratio of the laser's spectral intensity to that of the adjacent ASE being $>8 \times 10$ (Refs. 4 and 5). Nearly all the ASE resulted from the amplification process. The pulses had a median duration of 6 ns (FWHM) and an average input pulse energy of ≈ 1.5 mJ as measured with a thermopile (Eppley Labs). The transverse spatial profile of these pump pulses was well filtered to produce a nearly gaussian distribution. A well-defined column of excited atoms was assured for Ca densities of 10^{11} - 10^{14} cm^{-3} since the pump beam fluence (photons/ cm^2) was sufficient to "burn" completely through the 50-cm column.

The IR emissions from the cell were studied either with a commercial Ge:Au crystal mounted in an LN_2 dewar (Judson) or a Ge:Hg detector which was mounted to a home-built transmission line that was mounted, in turn, to a single stage Gifford-McMahon cryorefrigerator (Cryomech). The latter had a $D^* > 1.5 \times 10^9$ ($\text{cm Hz}^{\frac{1}{2}} \text{W}^{-1}$) at the wavelengths studied and bandwidth in excess of 350 MHz.

This noted value is probably an underestimate of the detector's true speed in the mid-IR. The analysis was limited to using the 1.06 μm emission from an Nd:YAG laser operating near threshold as a source of modulated light. Estimates were made of the detector's bandwidth from Fourier transforms of its response to this short λ radiation. The limitation of this analysis occurs because 1.06- μm radiation is detected near the front surface of the photoconductive crystal, while the mobilities of the charge carriers are faster in the bulk sample where mid-IR radiation ~ 4 -8 μm would be detected. Figure 4 shows an A-B comparison of the 1.06- μm signal measured simultaneously with a high speed Si-PIN photodiode (bandwidth limited to 500 MHz) and the Ge:Hg detector system.



time (5 ns/div)

Figure 4. An A - B comparison of IR detector and fast photodiode to 1.064 μm radiation. (A shows the response of the photodiode with a bandwidth limit of 500 MHz, while B shows the response of the IR detector.)

The output of this detector was connected directly to either a 500-MHz analog oscilloscope or a 1GS/S digitizing oscilloscope (DSO-one channel of a Tektronix DSA602) with a matched 50- Ω coax cable. Occasionally, it was necessary to amplify the signal with a 30-dB (1-500 MHz) preamplifier connected near the detector. The pump pulse, any conical emissions, and the optical SF pulses were monitored with a fast photodiode (1.8-GHz Opto-Electronics) or PMT. Many of the IR and optical SF emissions could be readily separated with bandpass filters, but the option of studying the emission spectrum with a 0.75-m grating monochromator was also available.

The absolute yield of photons was measured with an LiTaO_3 pyroelectric detector (Molelectron) which was calibrated against the thermopile (the thermopile had an absolute accuracy of $\pm 2\%$ traceable to NIST standards). The accuracy of this secondary calibration was assessed at ± 15 percent. The apparent large error in transferring an absolute calibration results from the spectral composition of our spikey "calibration" laser pulses which have significant spectral contributions near the ~ 1 -GHz thermal 3-dB frequency of the front electrode of the pyroelectric detector. The thermal transfer function of the front electrode coating needs to be accounted for when analyzing extremely fast pulses. Relative measurements of the IR yields may be more precise, however, since they had longer and smoother temporal shapes than the "calibration" laser pulses.

The time average Stokes parameters of the transmitted pump laser and induced emissions were studied from a Fourier analysis of the transmitted signal through a wire grid polarizer. The wire grid polarizer and an MgF_2 Soleil-Babinet compensator (Karl Lambrecht) set at $\lambda/4$ were used to modulate the IR emissions by rotating their orientations successively through several rotations.

Facility to study the forward and backward emissions was achieved in one of two ways: by placing the Ge:Au detector and

polarization optics at either end, or when A-B comparisons of the IR pulse shapes were desired, a delay line was added to image both pulses on the faster Ge:Hg detector.

Absolute measurements of the excited state densities [$\text{Ca}(4\ ^1\text{P}_1)$] and [$\text{Ca}(3\ ^1\text{D}_2)$] were made to verify the IR quantum yield measurements. These densities were measured by the equivalent width technique using the highly attenuated light from a second tunable pulse laser oscillator. This laser was scanned over the $4s4p\ ^1\text{P}_1-4p^2\ ^1\text{S}_0$ transition at 5512 Å and the $3d4s\ ^1\text{D}_2-3d4p\ ^1\text{F}_3$ transition at 5349 Å (Fig. 5). By delaying this probe laser suitably with respect to the pump, the populations of these levels could be established before and after the evolution of the SF pulse. The spatial distribution of excited states was also studied by offsetting the probe laser. This allowed corroborating estimates of the Fresnel number F of the excited state distribution. The Fresnel number of the excited state column is given as $F = A/\lambda L$ where A is the cross sectional area of the cylinder, L is its length, and λ is the wavelength of the SF emission. The Fresnel number is an important parameter which determines whether the medium acts mostly as a one-dimensional system or will have transverse modes. In order to reduce the issues of propagation, the system is arranged to have $F = 1$ since $F < 1$ will lead to significant diffraction losses and $F > 1$ will lead to higher off-axis modes. (The number of off-axis modes or Fresnel zones is $\approx F^2$ [Ref.7]). The Fresnel number F was also studied by measuring the IR divergence directly. In general these two methods agreed within 25 percent.

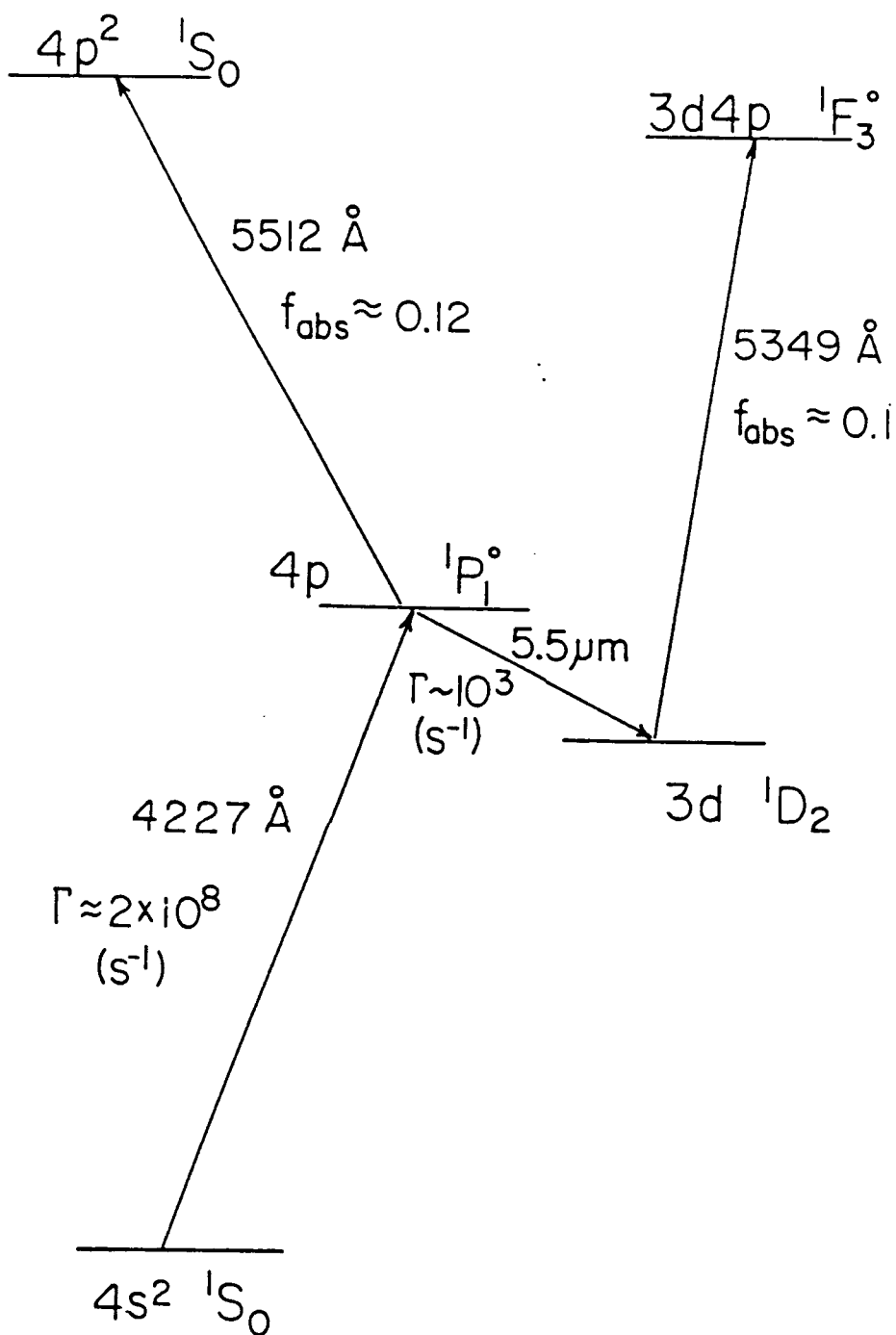


Figure 5. Partial term diagrams for Ca pump and probe scheme.

3.0 SPECTROSCOPY OF Ca AND Sr VAPOR

Figure 1 shows a partial level scheme for Ca of the levels below its principal resonance 1P_1 state. The level scheme for Sr is quite similar since various spectroscopic studies of these systems indicate that they are analogs. Nearly the entire optical oscillator strength of each atom (≈ 2 by the Thomas-Reiche-Kuhn sum rule) is possessed by the principal transition out of the ground state (~ 1.98 for Ca and 1.96 for Sr). Such large oscillator strengths assure that these transitions will be optically trapped even at moderate atomic densities $>10^{11} \text{ cm}^{-3}$. Thus, when these transitions are pumped by a pulse laser, they remain trapped for periods $\sim 1 \text{ } \mu\text{s}$ for densities $>10^{12} \text{ cm}^{-3}$. Likewise, radiative diffusion is slowed substantially so a well-defined column of excited atoms can be created, and its spatial distribution is retained for much longer than the $\sim 5\text{-ns}$ radiative lifetime. Since the branching ratio to the lower lying 1D_2 state is about 10^{-5} of the principal resonance line, one expects radiative transfer to this state to be small. In fact, it is the long optically trapped lifetime of the 1P_1 states which abets the cooperative transfer by SF to the 1D_2 state.

Further, it has been shown in Ca (Ref. 8) and in Sr (Ref. 9) that direct spin changing collisional transfer out of 1P_1 to the lower lying 3D_J levels is fairly substantial in the presence of the rare gases. A consequence of this surprising behavior is the possibility to create an inversion between the 3D_J and $^3P_{J-1}$ states. In fact, characteristic delayed emissions were observed on these transitions which were established to be SF rather than ASE. The identifications of the emission mechanisms are made in the next section.

Note, however, that the observations of SF on the 1P_1 - 1D_2 transitions of Ca and Sr are highly analogous to similar observations first made in Cu-vapor lasers operated near threshold. This suggests that one could readily replace the

mechanism of population transfer to the principal 1P_1 resonance level by electron impact and thus expect to produce fixed wavelength pulsed light sources in the mid-IR. This possibility has not yet been tested experimentally, but the results presented in the next section suggest that the quantum yields for SF emission could be quite high. In the presence of a rare gas buffer charge, Ca(4^1P_1) and Sr(5^1P_1) will also transfer rapidly to their respective 3D_J levels. The SF or stimulated emissions on the 3D_J - $^3P_{J-1}$ transitions could be used as sources of ~ 1.95 - and ~ 2.9 - μm radiation for the cases of Ca and Sr, respectively.

The actual spectroscopy of the Ca(4^1S_0 - 4^1P_1 - 3^1D_2) Raman level scheme (and its analog in Sr) is actually quite complicated in the presence of a strong pump field.

The principal resonance transition (1S_0 - 1P_1) will split into a pair of doublets in the presence of the pump laser. The Autler-Townes splitting and associated level shifts of the resulting dressed states are shown in Figure 6 for a blue detuning of the pump laser. The role of the "virtual" and real levels is reversed for a red detuning. The size of the AT-splitting is given in terms of the generalized Rabi rate Ω' (also referred to as the optical nutation rate). The size of this is parameterized in terms of the Rabi rate χ and the laser detuning from the (field-free) atomic transition Δ as $\Omega' = [\chi^2 + \Delta^2]^{\frac{1}{2}}$. The strength of the light field interaction χ is given as $\chi = \mu E/\hbar$ where E is the semiclassical field strength of the pump laser and μ is the dipole matrix element of the transition. The quantity E is related to the pump laser irradiance $I(\text{W}/\text{m}^2)$ by $I = \frac{1}{2}c\epsilon_0|E|^2$. For the case of the Ca or Sr principal resonance transitions, an incident monochromatic laser irradiance of $100 \text{ MW}/\text{cm}^2$ will yield a Rabi rate $\chi \approx 20 \text{ cm}^{-1}$ ($3 \times 10^{11} \text{ s}^{-1}$). For comparison, a 1-2 mJ, 6-ns pump laser collimated to ~ 1 -mm diameter can produce Rabi rates comparable to 10 cm^{-1} .

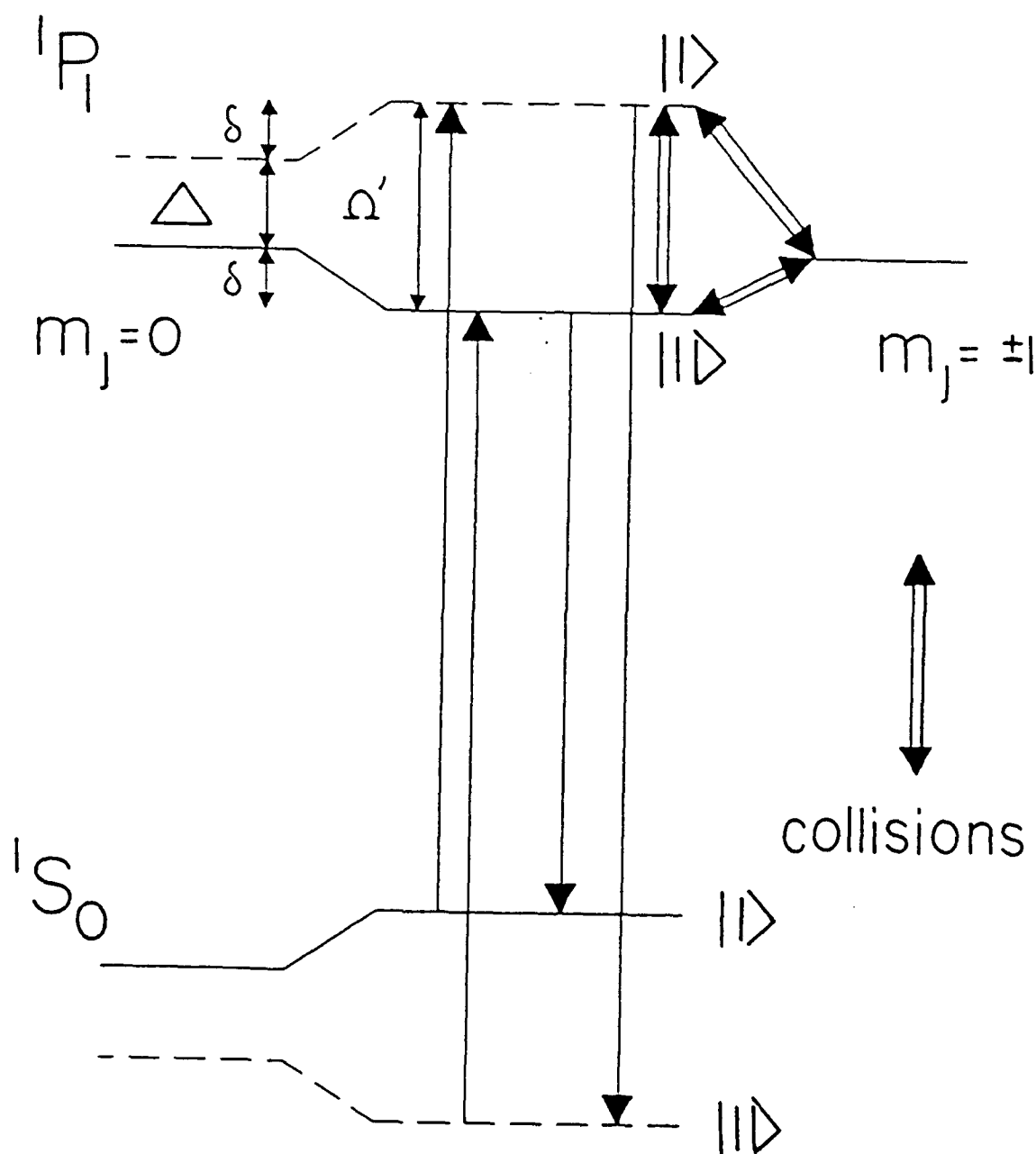


Figure 6. Dressed states of $\text{Ca}(4\ ^1S_0 - 4\ ^1P_1)$ transition in the presence of a strong laser field. (The "virtual" dressed states are denoted by the dashed lines; radiative transitions by solid lines and collisions by double solid lines. In the presence of a polarized laser only the $M_J = 0$ level is split.)

Raman scattering from the dressed level $|I_{N+1}\rangle$ to the final 1D_2 state is expected to generate stimulated emission at the Stokes frequency $\omega_L - \omega_{12} - \delta$ where ω_{12} is the field-free atomic level separation of the 1P_1 - 1D_2 transition and δ is the ac Stark shift of the 1S_0 - 1P_1 transition. This emission was the incentive for this work since it is tunable. A sequence of three- and four-photon scatterings can also take place through the "virtual" dressed levels. The three-photon scattering will populate the $|II_{N+1}\rangle$ dressed state which will lead to fluorescence at $\omega_{10} - \omega_{20} + \delta$ in the duration of the laser pulse. This leads to the well-known Mollow triplet of fluorescence signals in a strictly two-level system. In the presence of collisions, the dynamics of this population transfer are modified further (Ref. 6).

Raymer and Carlsten (Ref. 10) were first to discuss how both the Raman and induced fluorescence near ω_{12} can become stimulated at sufficiently high pump intensities. The competition and interplay of the Raman scattering and direct fluorescence to the final 1D_2 state was later reexamined theoretically in more detail (Refs. 11 and 12).

The general important result of the work was the observation that SRS never achieves sufficient gain to produce a measurable emission. Instead, a time delayed emission at the fixed wavelength of the 1P_1 - 1D_2 transition is observed in each case for Ca and Sr. The difficulties of generating tunable SRS on the electronic Raman transitions 1S_0 - 1P_1 - 1D_2 , involving the principal resonance, are perhaps intrinsically unachievable with just one pump laser. The magnitude of the oscillator strength for the 1S_0 - 1P_1 transition is so large that other spontaneous scattering processes will always overtake the initiation of SRS by spontaneous emission. In particular, the three-photon scattering from the virtual dressed state $|I_{N+1}\rangle$ will readily lead to transfer into $|II_{N+1}\rangle$ in the case of Ca and Sr.

4.0 ELECTRONIC EXCITATION AND RELAXATION OF $\text{Ca}(4^1\text{P}_1)$ AND $\text{Sr}(5^1\text{P}_1)$

4.1 SUPERFLUORESCENCE FROM $\text{Ca}(4^1\text{P}_1)$

This experiment consisted of measuring the populations of the three-level system, the absolute IR photon yield, and temporal pulse shapes for various ground state densities in the range of 10^{11} - 10^{14} cm^{-3} . Most of these studies were performed at a buffer gas pressure of 1 Torr. The effects of collisional redistribution and dephasing were also studied over a range of pressures extending up to ~800 Torr.

The ground state density was controlled by the saturated vapor pressure of Ca along a uniformly heated 50-cm-long section bounded by knife edge baffles. Figure 7 compares the equivalent width measurements to the ground state vapor pressure estimations. Typically, these two determinations matched within 35 percent.

The vapor column of length L was excited in what is referred to as longitudinal pumping by launching the pump pulse along the axis of the cell. This type of excitation is expected to produce an asymmetry between the amount of forward scattered and back-scattered emissions. Generally, it is expected that the gain for stimulated forward scattering will be much greater in this case because the pump pulse and medium polarization travel forward at nearly the same velocity and in phase. If the pump pulse has considerable structure, or its transit time $\tau_E = L/C$ is large or comparable to its duration τ_p , then the backscattered emission will usually not remain in phase with the pump pulse so the nonlinear gain for backscattered amplification is smaller. Typically, this asymmetry of gain can be one order of magnitude, or more, different.

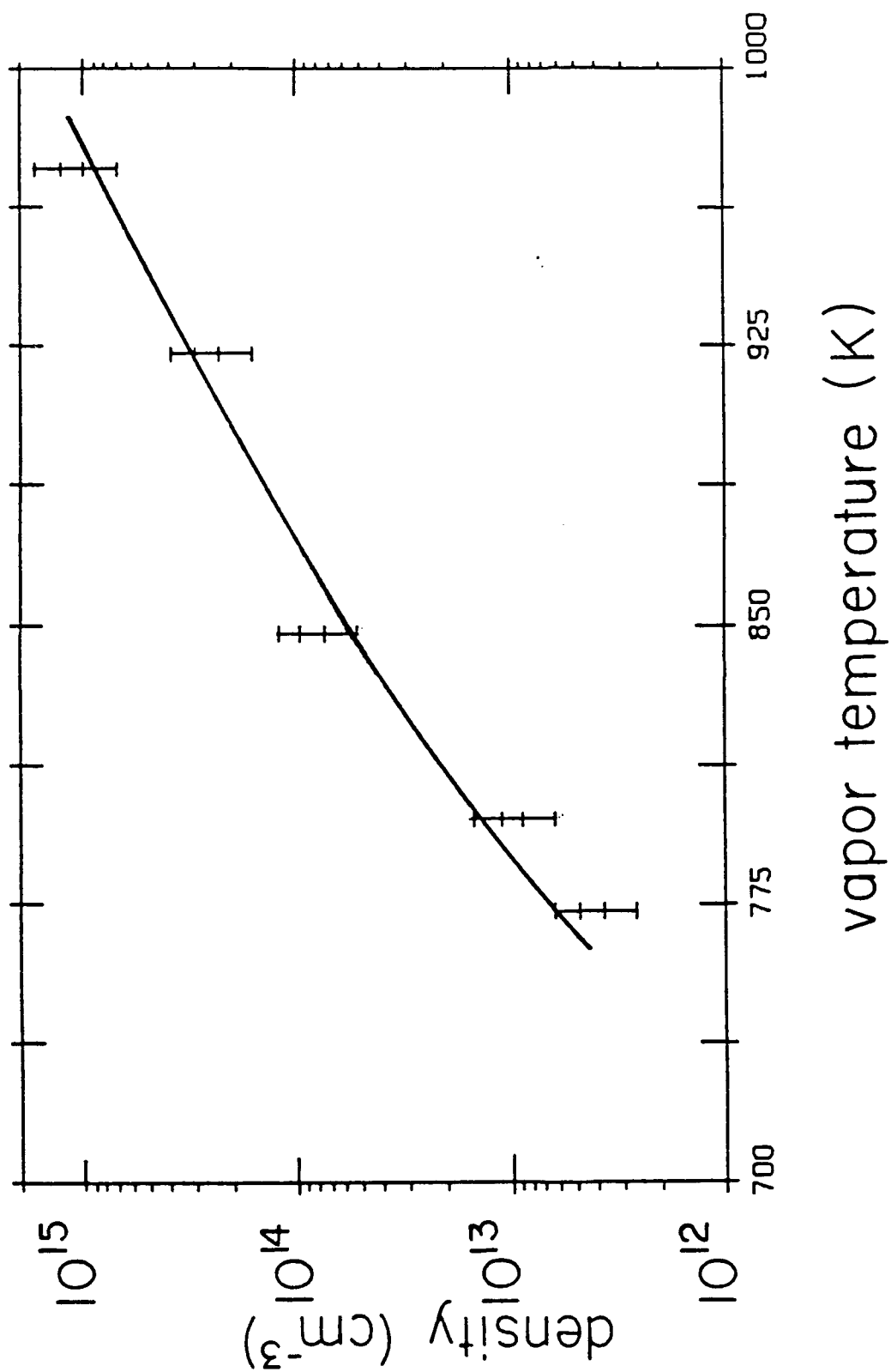


Figure 7. Comparison of a ground state $[\text{Ca}(1S_0)]$ by the technique of equivalent width with saturated vapor pressure curve.

The initial studies looked at the spectral composition of the IR emission(s) as a function of pump laser detuning and for evidence of this forward-backward asymmetry. For $[\text{Ca}(^1\text{S}_0)] < 2 \times 10^{14} \text{ cm}^{-3}$ and low Ar buffer pressures < 5 Torr, just the fixed emission at $5.5 \text{ }\mu\text{m}$ was observed. These IR pulses always had delays $\geq 13 \text{ ns}$ as measured from the beginning of the pump pulse (see Fig. 8 for representative signals). The lower bound is significant since this was the total duration of the pump laser. This observation would imply that SRS was not induced since it must occur during the duration of the pump laser. If the density of Ca vapor was increased to $> 2 \times 10^{14} \text{ cm}^{-3}$, then IR emissions occurred under the pump pulse, but after careful spectroscopic study it was found that all such emissions were the result of cascade SF (or SRS) emissions occurring from two-photon excited Rydberg levels. The 0.75-m monochromator with a 10-cm -wide, $75\text{-}\ell/\text{mm}$ grating blazed for $10 \text{ }\mu\text{m}$ had sufficient resolution in second and third order to easily resolve the SF and any SRS emission near $5.5 \text{ }\mu\text{m}$ for pump detunings greater than twice the Rabi rate. In general, the IR emissions were sufficiently intense ($\sim 2 \text{ }\mu\text{J}$ when $\Delta = 0$ in the forward direction) so that the monochromator could be operated with a practical resolution $> 6,000$ in second order while achieving throughputs of > 30 percent. The spectrum of the $\sim 5.5\text{-}\mu\text{m}$ emissions were studied for a variety of laser detunings as large as $\pm 150 \text{ cm}^{-1}$ and no evidence of tunable SRS was ever observed. However, detectable SF emissions were produced for detunings as large as $\pm 75 \text{ cm}^{-1}$. This is a sufficiently large detuning to consider the pumping process as off-resonant.

The delay times τ_p for these SF-like (i.e., time delayed) pulses range from 13 ns at $[\text{Ca}(^1\text{S}_0)] \sim 10^{14} \text{ cm}^{-3}$ to as much as $60\text{--}70 \text{ ns}$ at the lowest ground state densities studied ($\sim 2 \times 10^{11} \text{ cm}^{-3}$). The former conditions produced IR pulses with total energies $\sim 2 \text{ }\mu\text{J}$ in the forward direction. Similar pulse energies ($\sim 1.5 \text{ }\mu\text{J}$ for the highest densities) and pulse shapes were observed in the backward direction. Figure 9 shows an example of the forward and time delayed backward emission as measured by the same Ge:Hg detector.

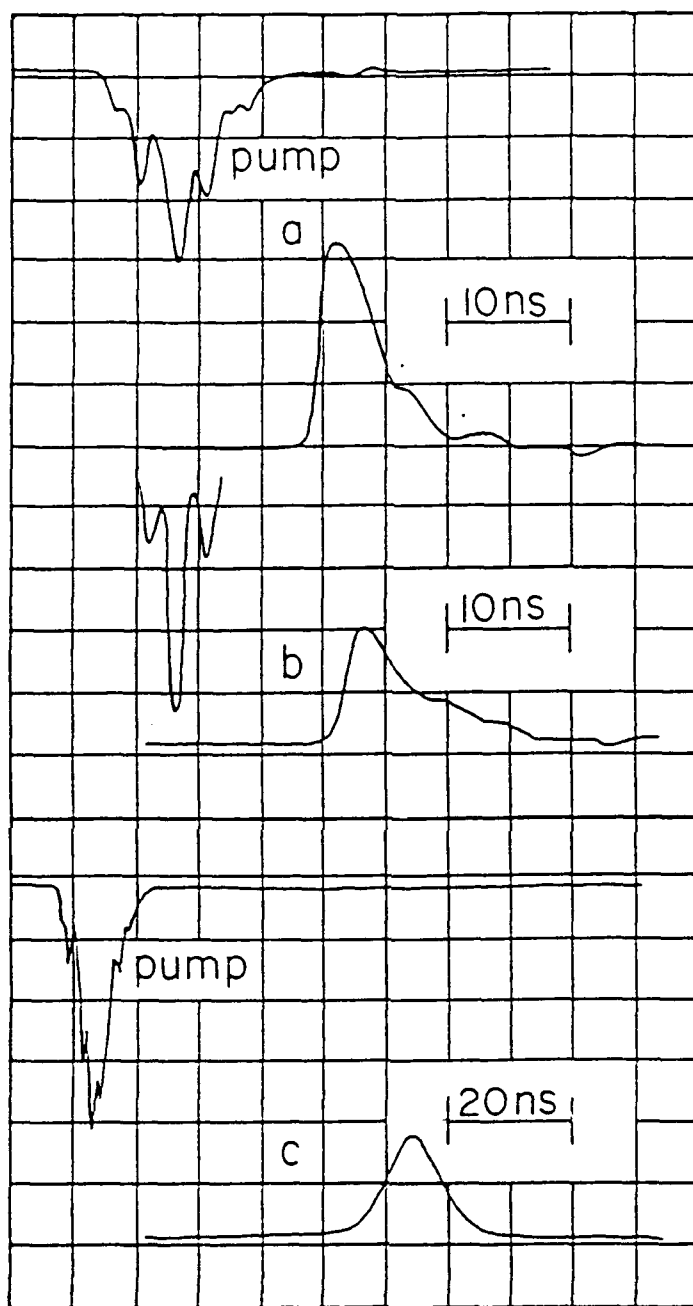
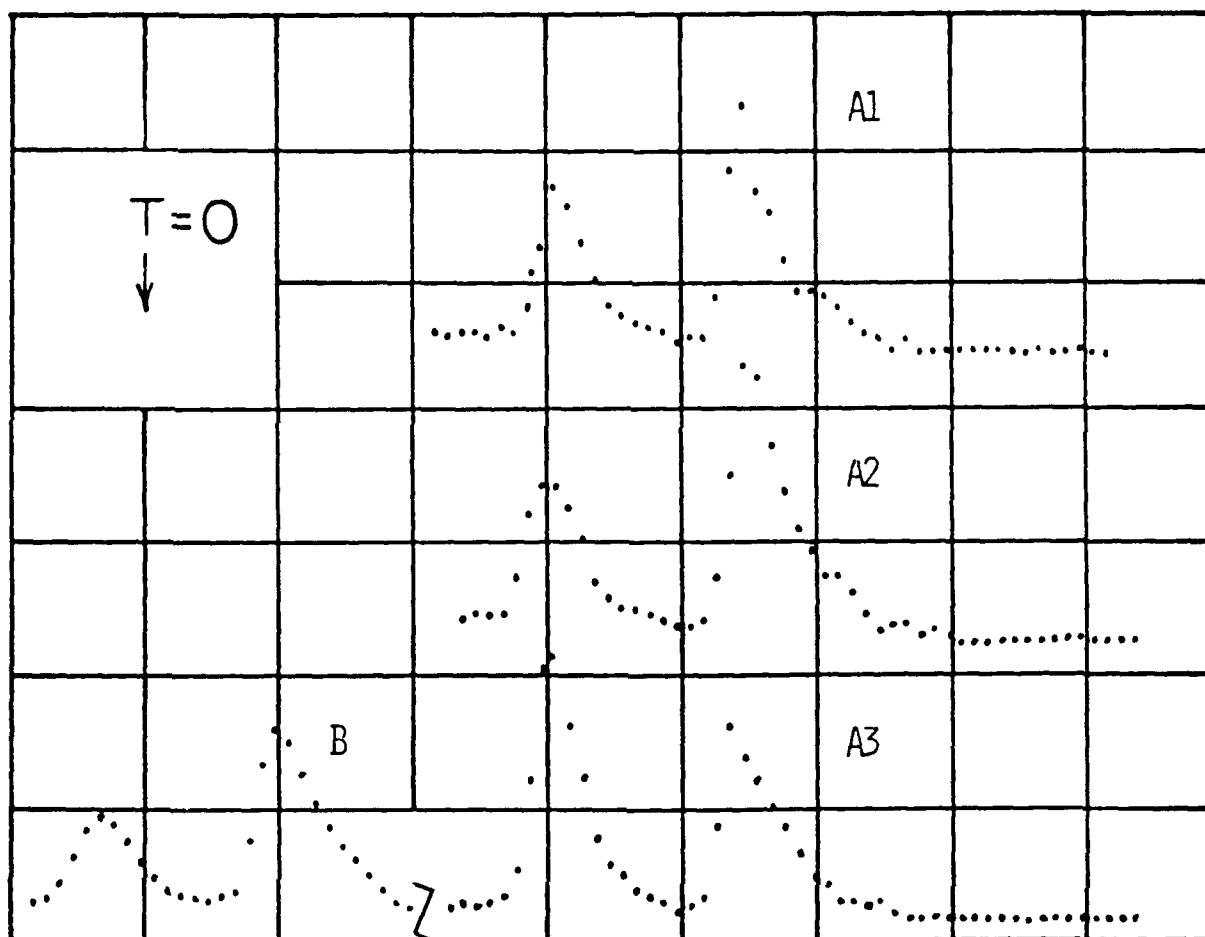


Figure 8. Representative SF pulses at $5.5 \mu\text{m}$. (A shows the response pulse shape for conditions of high laser intensity and resulting high excited state density; B and C show cases of decreasing excited state density, respectively.)



time (10 ns/div)

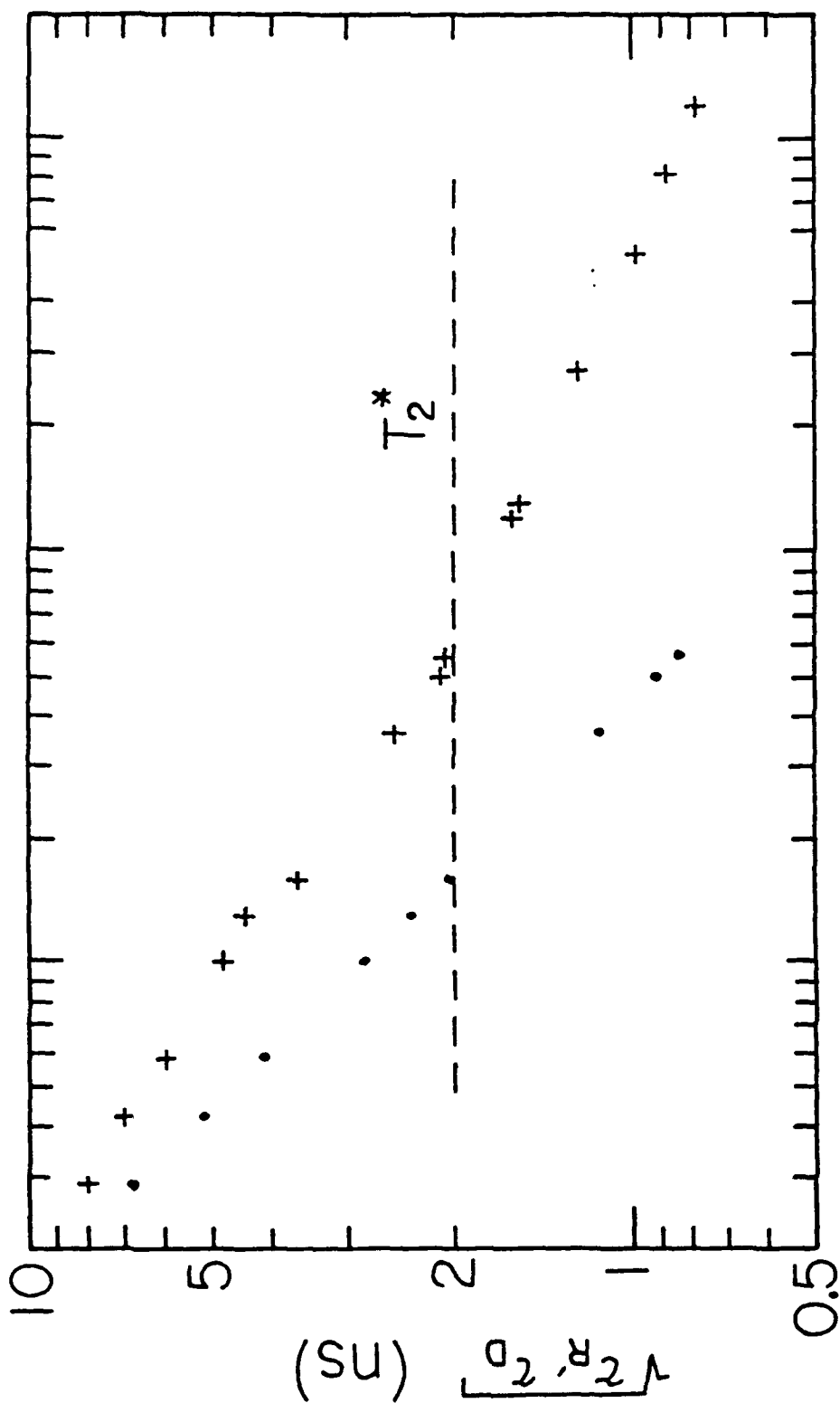
Figure 9. Comparison of forward and backward scattered SF emission pulse shapes. (A1 - A3 show several single shot traces of the forward and backward scattered pulses; note that the optical delay was 16 ns which matches the electronic delay within 2 ns. B shows the time average of 2000 shots. The conditions of excitation led to a 30-ns delay time for onset of the SF.)

There are two unexpected results of these observations. First is the existence of SF with delay times substantially longer than the natural radiative lifetime T_N of the $\text{Ca}(4^1P_1-4^1S_0)$ transition ($T_N \approx 4.6$ ns). Apparently even in the presence of rapid dipole dephasing by radiative redistribution, SF is an effective mechanism to radiatively cool the sample. Consider that the homogeneous dipole dephasing time T_2 ($T_2 = 2T_N$ in the absence of collisions) will be further reduced by the effects of Doppler broadening. Then T_2^* is evaluated to be $(T_2^*)^{-1} = T_2^{-1} + \Delta\nu_{\text{Doppler}}/0.44$ or $T_2^* < 2$ ns. Here $\Delta\nu_{\text{Doppler}}$ for the SF transition is estimated to be 190 MHz at ~ 950 K. The T_2 and T_2^* are usually much smaller than the SF delay time τ_D .

It has been proposed theoretically (Ref. 13) that SF emission is possible only when $T_2^* > (\tau_R \tau_D)^{1/2}$ where τ_R is the radiative coupling time for SF to develop. The τ_R is historically taken to be (Ref. 3)

$$\tau_R = \frac{8\pi A T_{12}}{3\lambda^2 N}$$

where T_{12} is the radiative lifetime of the SF transition, A is the cross sectional area of the cylindrical column, λ is the wavelength of the SF transition, and N is the total number of radiators that participate in the SF process. In these situations τ_R range from $\sim 10^{-9}$ s at the lowest densities to $\sim 10^{-12}$ s at the higher densities. Figure 10 shows a comparison of the quantity $(\tau_R \tau_D)^{1/2}$ versus the experimentally determined number of $\text{Ca}(4^1P_1)$ atoms left after the passage of the pump laser. A modified value of $(\tau_R \tau_D)^{1/2}$ is also shown; this is determined by assuming that only a subset of atoms in a column length L_C given by the Arecchi-Courtens condition can initially participate (Ref. 14). This maximum cooperation length is usually shorter than the total column length L since atoms at one end must be able to communicate with atoms at the other end during the evolution of the system. It is expected then that the



total IR yield (# of photons)

Figure 10. Comparison of SF evolution time $(\tau_R' \tau_D)^{1/2}$ with T_2^* as a function of the number of SF radiators N . (N is measured from the absolute photon yields. + denotes data corrected for the Arecchi-Courten's cooperation length while . assumes the entire column length participates.)

total path length of excited atoms will consist of several independent zones where SF evolves separately. Gross and Haroche (Ref. 15) have proposed that the number of independent slices is of order $L/L_C = (\tau_E/\tau_R)^{1/2}$, where $\tau_E = L/C$ is the transit time of the entire column. For this proposition to hold, the evolution time of each section is then taken to be $\tau_{R'} = (\tau_R\tau_E)^{1/2}$.

It is seen that the pulses with greatest delays do not satisfy either $T_2^* > (\tau_R\tau_D)^{1/2}$ given for the whole sample length or the modified condition $T_2^* > (\tau_{R'}\tau_D)^{1/2}$.

A possible explanation for the existence of such SF pulses undergoing Doppler dephasing might follow if only a single-velocity group participates. If this is the case, then presumably $T_2 \approx 2T_N$ would obtain for a single-velocity group. Studies by Maki, et al., have shown that when the homogeneous dipole dephasing $T_2 < (\tau_R\tau_D)^{1/2}$, then the SF emission reverts to ASE (Refs. 16 and 17).

Maki and coworkers were also able to theoretically model this transition to ASE (Refs. 16 and 17). We modified this model in the context of the Ca SF experiment to account for the effects of radiation trapping by using a time varying number density of excited states which mimics the effects of radiation redistribution. Since the SF delay time τ_D is long compared to the natural lifetime T_N , a number of absorption and emission events occur on the optically thick 1P_1 - 1S_0 transition while the SF evolves. This results in radiation redistribution into the SF velocity group and allows the remainder of the velocity groups to contribute indirectly to the emission. This velocity reshuffling is shown to partially damp out the temporal ringing associated with SF. Some results of this model are shown in Figures 11 and 12. Figure 11 shows several different single shot realizations of the modeled SF for the conditions with $[Ca(^1P_1)] \sim 10^{13} \text{ cm}^{-3}$. Figure 12 shows that changes in the rate of velocity group reshuffling (due to radiative redistribution) do indeed destroy

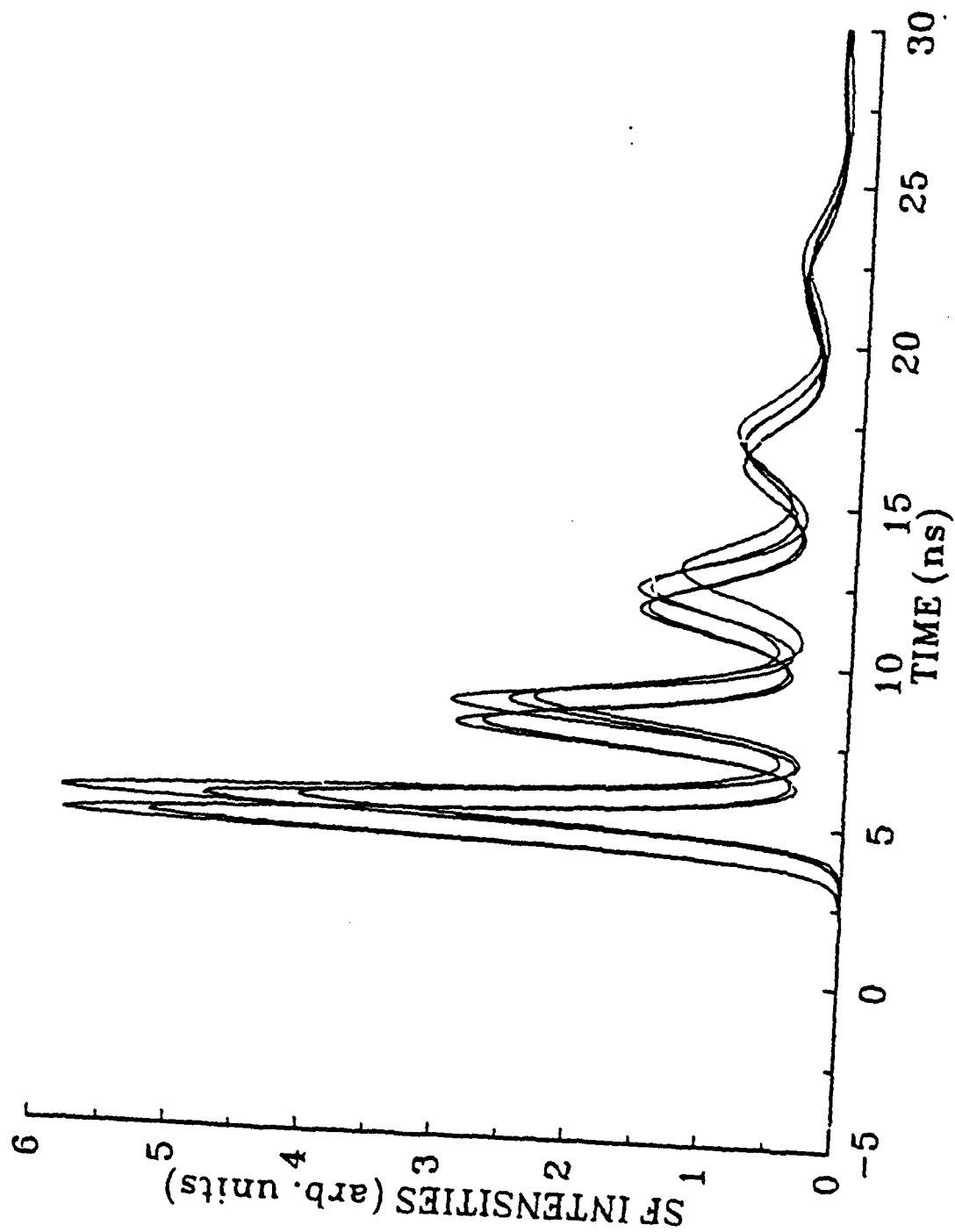


Figure 11. Model calculations of SF - single shot realizations. (The calculations assume an excited state density of 10^{13} cm^{-3} and a radiative relaxation time of 9 ns.)

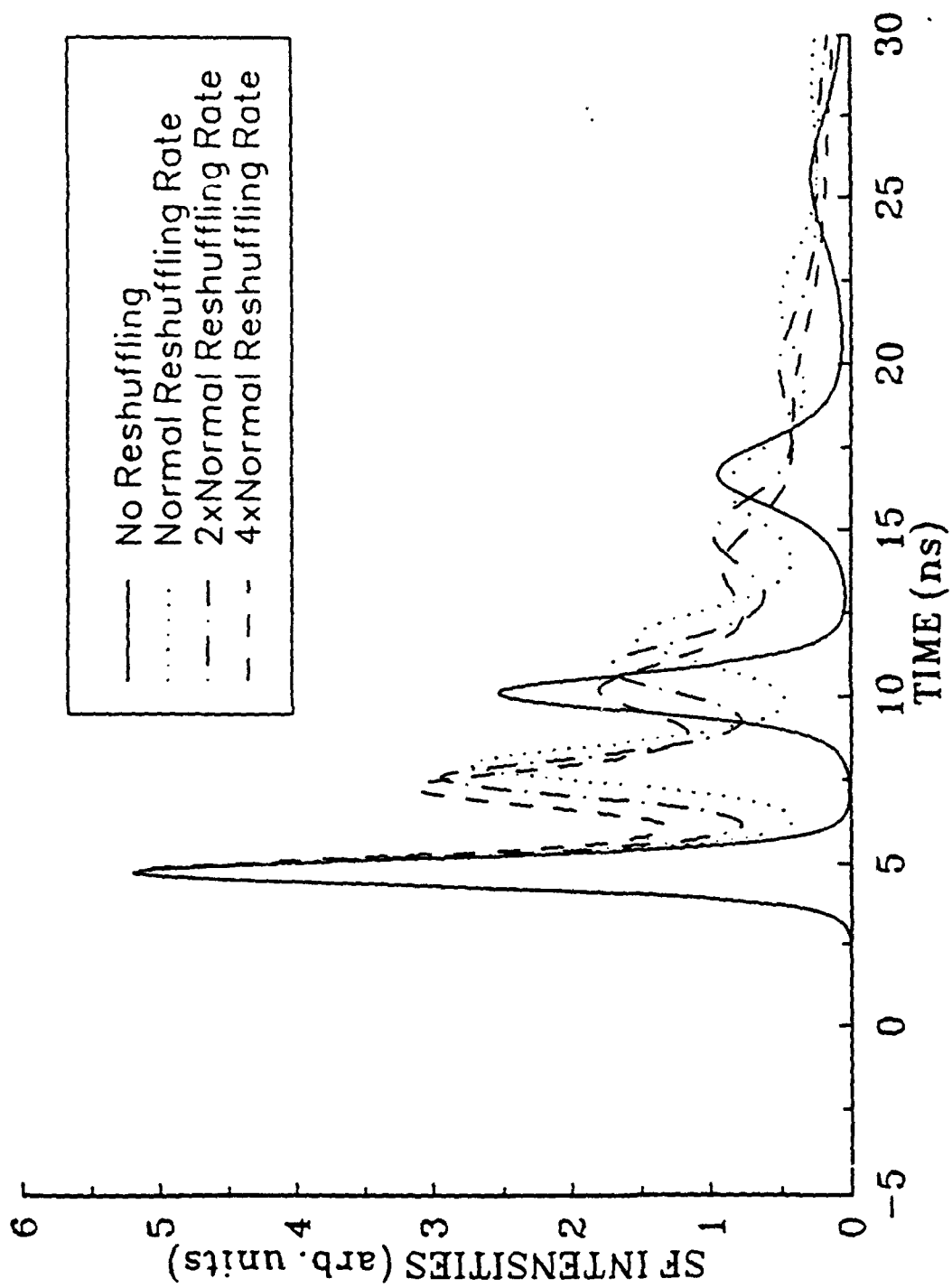


Figure 12. Model calculation of SF for different rates of radiative redistribution. (Normal is taken to be $1.1 \times 10^8 \text{ s}^{-1}$.)

the observed modulation of the SF ringing. This is a new facet of a longstanding problem in the modeling of SF. In general, the experimentally observed SF signals show less ringing than theoretical predictions; however, effects of velocity group reshuffling, either by collisional or radiative transfer, were not considered explicitly before this work.

The quantum yield of SF to produce IR was also surprising. It was discovered that >90 percent of the excited 1P_1 population left after the pump laser was transferred into the 1D_2 state by the SF emission. Superfluorescence is a cooperative emission process, so just as superradiance, it has the potential to fully empty the reservoir of excited states. Even SF pulses with time delays >50 ns were releasing ~90 percent of the excited state 1P_1 density. These observations were performed by measuring the absorption from the 1P_1 and 1D_2 states before and after the SF emission. This feature of SF has apparently not been treated by current theory which models SF as a stimulated emission process. The results are currently being reinvestigated more carefully to check this unusual result.

4.2 COLLISION-INDUCED SF BY SPIN-CHANGING COLLISIONS WITH RARE GASES

There has been considerable interest in storing energy in the lower lying electronic states of Group IIA elements in the hope of achieving laser action, either out of these levels or by collisional transfer in mixed metal vapors in analogy with the HeNe laser scheme. This section describes the investigations of SF emission near $\sim 1.95 \mu\text{m}$ due to the $\text{Ca}(3\text{d}4\text{s } ^3\text{D}_J\text{-}4\text{s}4\text{p } ^3\text{P}_{J-1})$ transitions. These SF emissions are a result of spin changing collisions which directly transfer population from the optically trapped $\text{Ca}(4 ^1\text{P}_1)$ levels to $\text{Ca}(3\text{d}4\text{s } ^3\text{D}_J)$. This unusual behavior by $\text{Ca}(4 ^1\text{P}_1)$ in the presence of rare gases is analogous to that in $\text{Sr}(5 ^1\text{P}_1)$ (Ref. 9).

Breckenridge and Merrow (Ref. 8) were the first to show that direct collisional deactivation of $\text{Ca}(4 ^1\text{P}_1)$ by the rare gases occurs predominantly ($>90\%$) to the lower lying $^3\text{D}_J$ states rather than to the nearer (and presumably spin preserving) $^1\text{D}_2$ state. An understanding of the reaction mechanism which allows this is still not in hand. Kelly, et al., then demonstrated analogous behavior in Sr by monitoring what was thought to be ASE on the $\text{Sr}(4\text{d}5\text{s } ^3\text{D}_J\text{-}5\text{s}5\text{p } ^3\text{P}_{J-1})$ transitions (Ref. 9). Subsequent, careful time resolved measurements by Gallagher and coworkers* have established that the rate coefficients for these spin changing collisions in Sr are substantial, e.g., $k(^1\text{P}_1\text{-}^3\text{D}_J) \sim 2 \times 10^{11} \text{ cm}^3 \text{ s}^{-1}$ for Sr interacting with Ar. The analogous rate coefficient for Ca-Ar is determined to be about (1/20) the result for Sr--this is slightly larger but consistent with relative estimates given by Wright and Balling (Ref. 18). The value is derived from an estimate of the population of $\text{Ca}(^3\text{D}_J)$ needed to achieve SF threshold compared to that for Sr. This estimate is not as reliable as measuring directly the time-resolved transfer, as was done in Sr by Gallagher, because it must assume a

* Dr. A. Gallagher, Joint Institute for Laboratory Astrophysics, private communication (1992).

transition rate for the $\text{Ca}(3^3\text{D}_J-4^3\text{P}_{J-1})$ transitions which is not reliably known.

Another interesting aspect of this work has been the discovery that these SF transitions in Ca produce strikingly clear ringing unlike all other SF experiments done to date. Figure 13 shows an example of this for the condition of low buffer gas density where only the $\text{Ca}(3^3\text{D}_3-4^3\text{P}_2)$ transition reaches threshold. The pronounced ringing is seen preserved even in the time averaged traces. This system has allowed one to study transverse effects of propagation such as the dependence of the temporal ringing with Fresnel number. The ringing is smeared when F is increased, either by changing the cross section of the pump volume or by raising the number of excited $\text{Ca}(3^3\text{D}_J)$ atoms so that the effective F of an independent slice is increased as the maximum cooperation length L_C is reduced. This work is ongoing, but it has helped clarify that the concept of a maximum cooperation length L_C is probably valid.

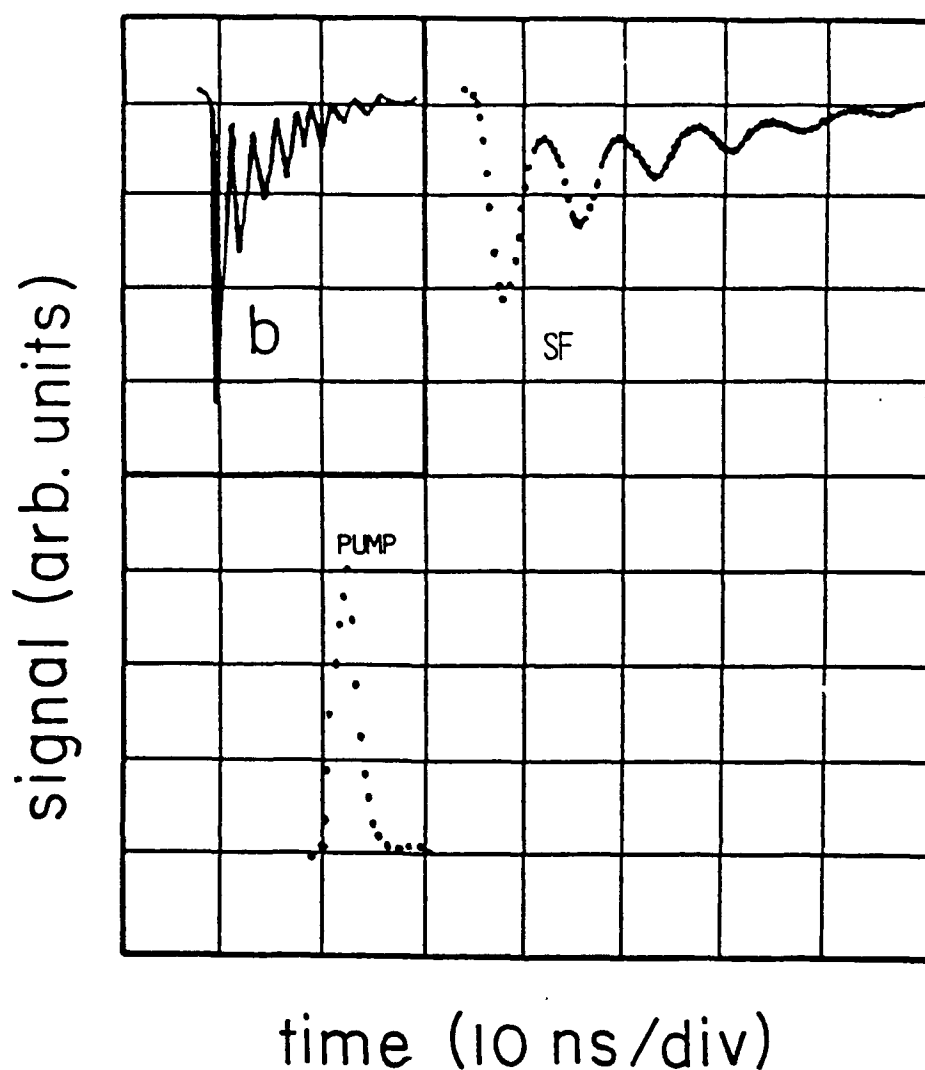


Figure 13. The SF emission of the $\text{Ca}(3^3\text{D}_3-4^3\text{P}_2)$ transition. (A time average of 2000 shots is shown on the right side while a single shot realization is shown in the inset marked b. Note that its time scale is compressed to 100 ns per division.)

4.3 MODIFICATION OF SF POLARIZATION BY COLLISIONAL REDISTRIBUTION OF RADIATION IN STRONG FIELDS

It has been anticipated that radiative cross sections for pressure broadened absorption will change substantially in the presence of a strong incident light field. Further, any strongly pumped transition will give rise to consequential scattering processes. These radiative transitions are modified in turn by quasi-elastic collisions that, in addition to collision-aided absorption, lead to a rich spectrum of collisional redistribution of the pump radiation. For example, if the transition occurs between states with spatial degeneracy, then collisional depolarization of the scattered or emitted radiation will occur.

In the presence of a strong pump field, radiative excitation never occurs via a single transition, but is assisted by collisions through a manifold of pathways--some of which are dynamically "created" by the intense light field (Fig. 14).

The strength of the light field interaction is parameterized in terms of the Rabi rate given by $\chi = \mu E / \hbar$, where E is the semiclassical field strength related to the pump intensity by $I = 1/2c\epsilon_0 |E|^2$ and μ is the dipole matrix element of the transition. The time scale for electronic response to the pump field is given in terms of the optical nutation frequency $\Omega' = [\chi^2 + \Delta^2]^{1/2}$. When Ω' is small so that $\Omega' \tau_c \ll 1$, where τ_c is the characteristic duration of a binary atomic collision, then the perturbation of the optically active atomic system is generated predominantly by the collision. In this so-called weak-field limit, traditional impact theory for pressure broadened absorption is suitable.

It is expected that strong field effects will occur when $\Omega' \tau_c \geq 1$. The field free or bare atomic levels then experience a substantial ac Stark shift and splitting $\sim \Omega'$ of the dressed levels in the duration of the strong excitation pulse.

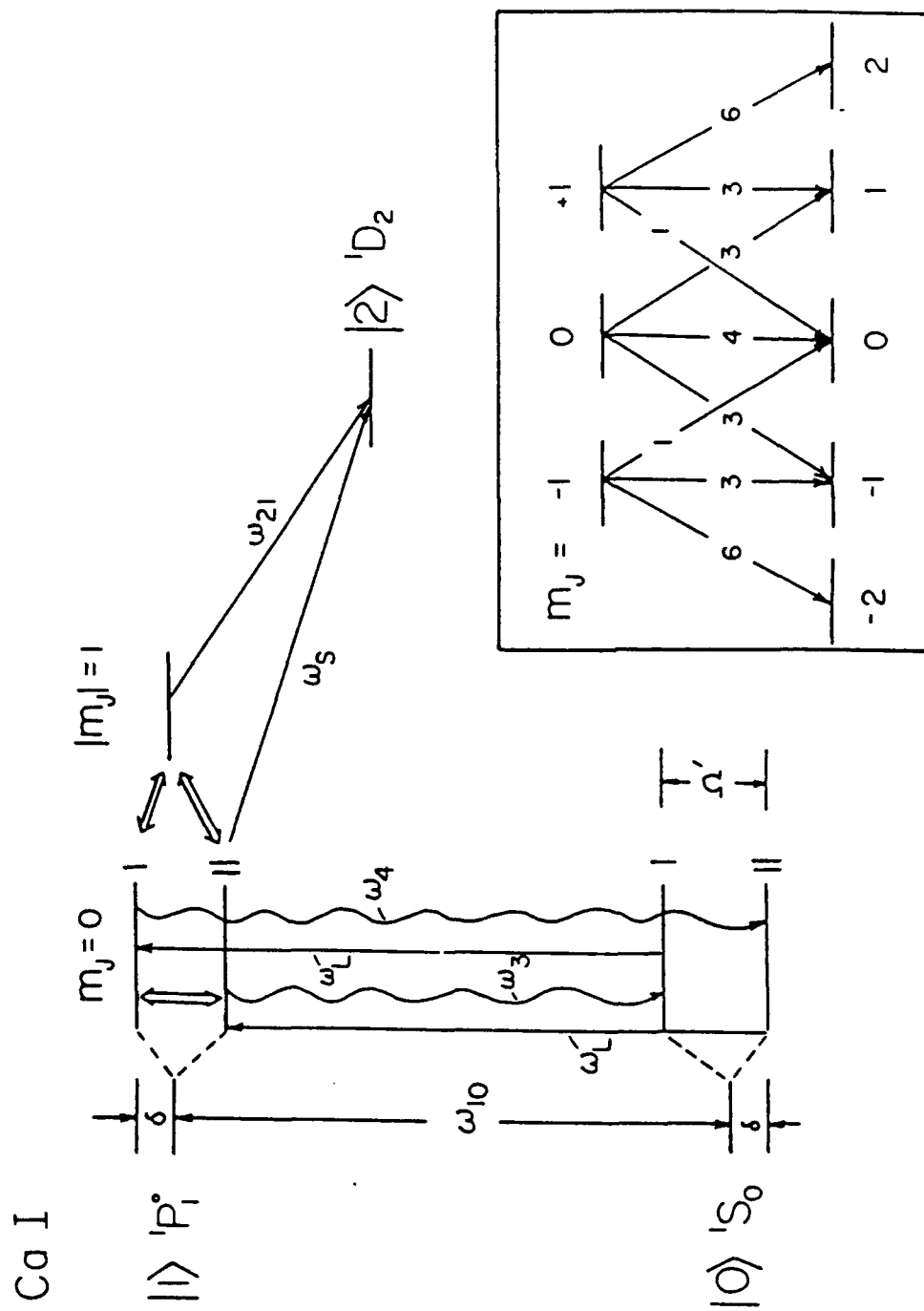


Figure 14. Collisional redistribution pathways for the dressed levels of a $1S_0-1P_1$ transition. (The scheme is shown for the case of a red detuning. The squares of the Wigner 3-J coefficients are shown in the inset for emission to the $1D_2$ states.)

Qualitatively then, the magnitude of the Stark shift and dynamic level splitting can vary significantly in comparison to the atom-atom interaction. It is possible that the level splittings can be sizable enough to affect the collisional transfer rates--even to the point of turning the rates off.

Szöke (Ref. 19) was first to realize this feature when he analyzed the studies of collisional redistribution in the Sr-Ar system pumped by a $\sim 100 \text{ MW/cm}^2$ pulse laser (Ref. 20). Light and Szöke (Ref. 5) noted that this scattering system is really a four-level system and that collisional depolarization between the m_J levels of the excited $\text{Sr}(^1P_1)$ state will also be modified by intense fields. Experimental studies by Kleiber, et al., (Ref. 21) of near resonant scattering and fluorescence involving $\text{Sr}(5^1P_1)$ perturbed by Ar have confirmed the essential features of the Light and Szöke model of optical collisions. Most notably, it was observed that the $\Delta m_J = 0$ transition "turns off" at high field strengths, while the $|\Delta m_J| = 1$ transitions (assisted by collisions) lead to significant depolarization of the redistributed radiation.

A new class of scattering-emission experiments which may become useful in further elucidating the role of optical collisions in strong fields is presented. Essentially an SF emission of IR radiation at ω_{21} which experiences a modification of its ellipticity of polarization is observed. The change in polarization is largely a function of the ratio χ/Δ ; for large detunings ($\chi/\Delta < 1$), the SF polarization is most nearly linearly polarized and parallel to the pump laser but switches orientation by 90 deg when $\chi/\Delta > 1$ (Fig. 15).

An analysis of the time averaged SF polarization was done by studying the Fourier harmonics of signal passed by a linear polarizer which follows a variable wave plate. In general, the SF intensity can consist of three contributions of polarization states I_L , I_C , and I_R due to radiation which is linearly,

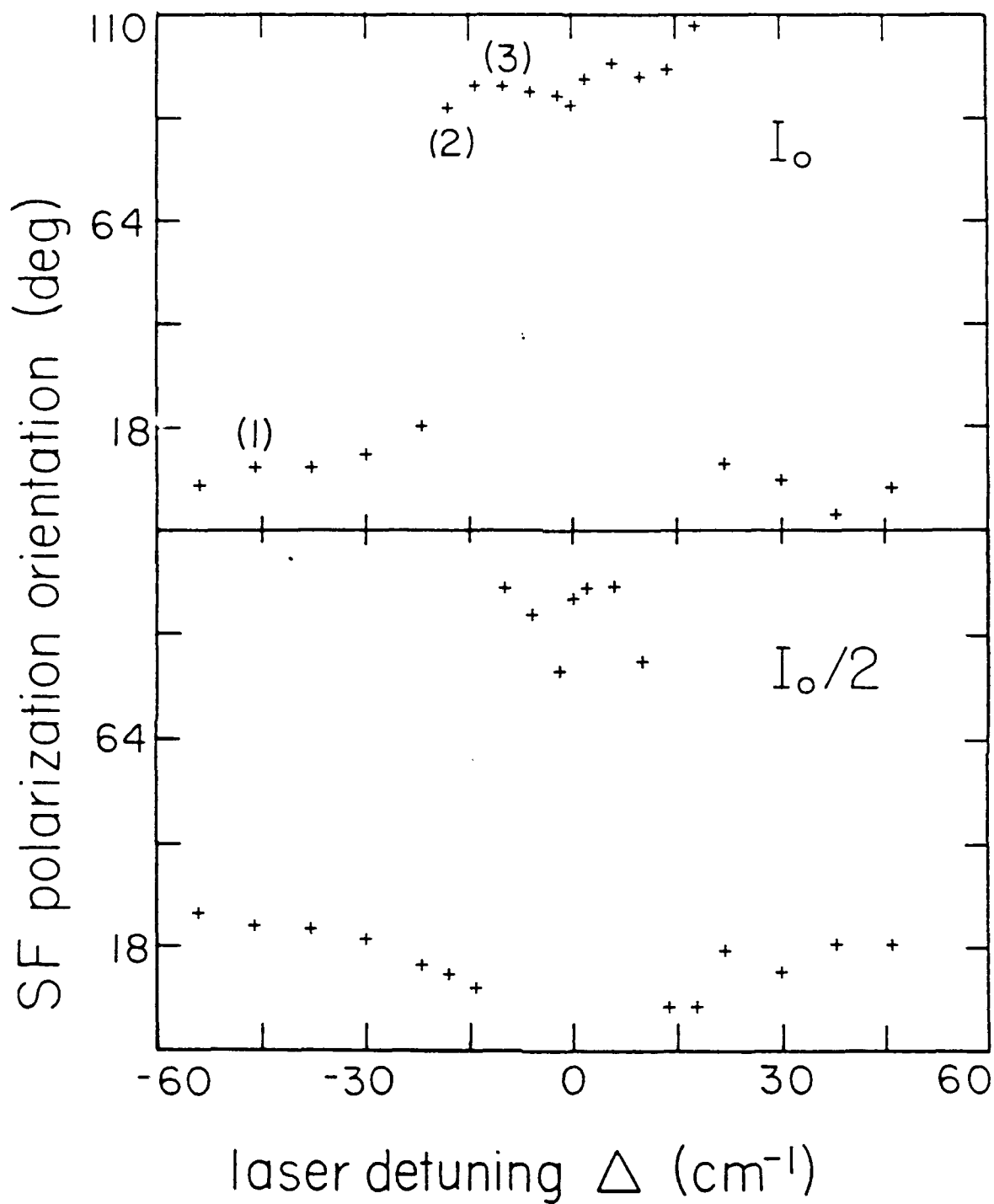


Figure 15. Orientation of SF ellipticity of polarization versus laser detuning. (I_0 corresponds to a laser irradiance of 100 MW/cm².)

circularly, or randomly polarized. Then the transmission function of the wire grid polarizer, in terms of its rotation angle θ , is given as

$$I_{SF} = I_L + I_C + I_R = A \cos^2 (\theta + \theta') + B$$

(Here $\theta_{SF} = -\theta'$ is the assigned angle of the polarizer θ for which the maximum time averaged peak height is recorded.) See Figure 16 for a typical example. The quantities $A + B$ and B denoted in Figure 16 represent the major and minor axes, respectively, of the ellipticity of polarization of the signal with respect to a defined laboratory orientation of the pump laser. The quantity A is the modulation of the $\cos^2(\theta + \theta')$ function and is a measure of the amount of linear polarization, whereas the quantity B is a measure of the circular and random contributions. The pump laser was >99 percent linearly polarized with its orientation vertical (defined here to be $\theta = 0$). Figure 17 shows an analysis of the response IR polarization for three different detunings Δ measured in the synthesis of Figure 15. It is apparent that the IR signal is fairly linearly polarized and parallel to the pump laser for large detunings, and its orientation flips for smaller detunings. The percentage of circular polarization (by rotating the $\lambda/4$ retardation element) was also studied, and its contribution was found to be <3 percent. Thus, the remaining portion of IR corresponded to mostly random polarization. At the position of the flip the IR emission was largely unpolarized.

This behavior is consistent with Light and Szöke's model (Ref. 5) and the calculations in References 6 and 21 which show that the $m_J = 0$ collisionally assisted transition is turned off when $x/\Delta > 1$, while the $|\Delta m_J| = 1$ optical collisions are still significant. The relative intensities and polarization of the SF signal, while not a direct measure of the populations of the dressed states, appear to provide a clear signature of the modification of the collision dynamics.

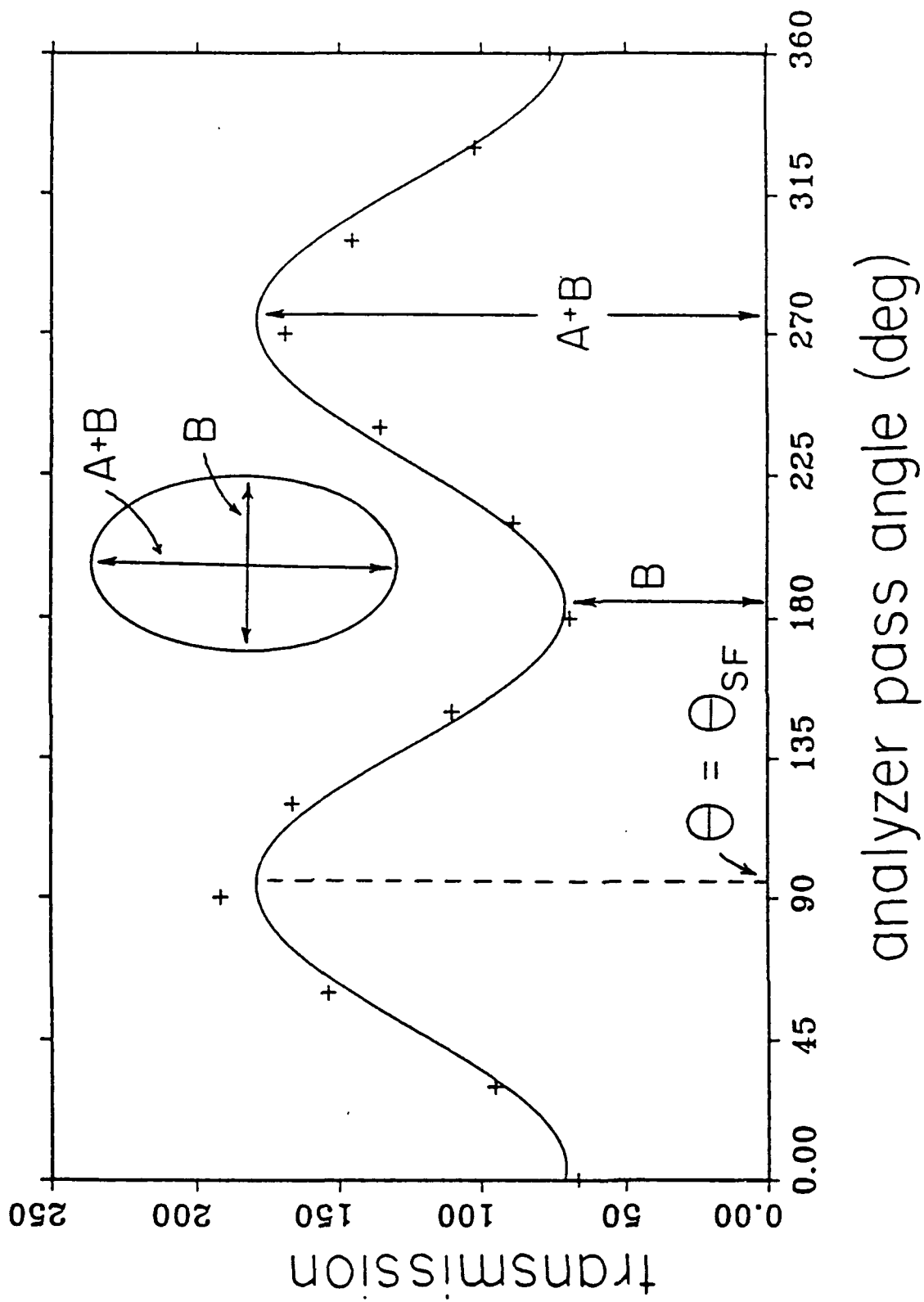


Figure 16. Analysis of SF ellipticity orientation.

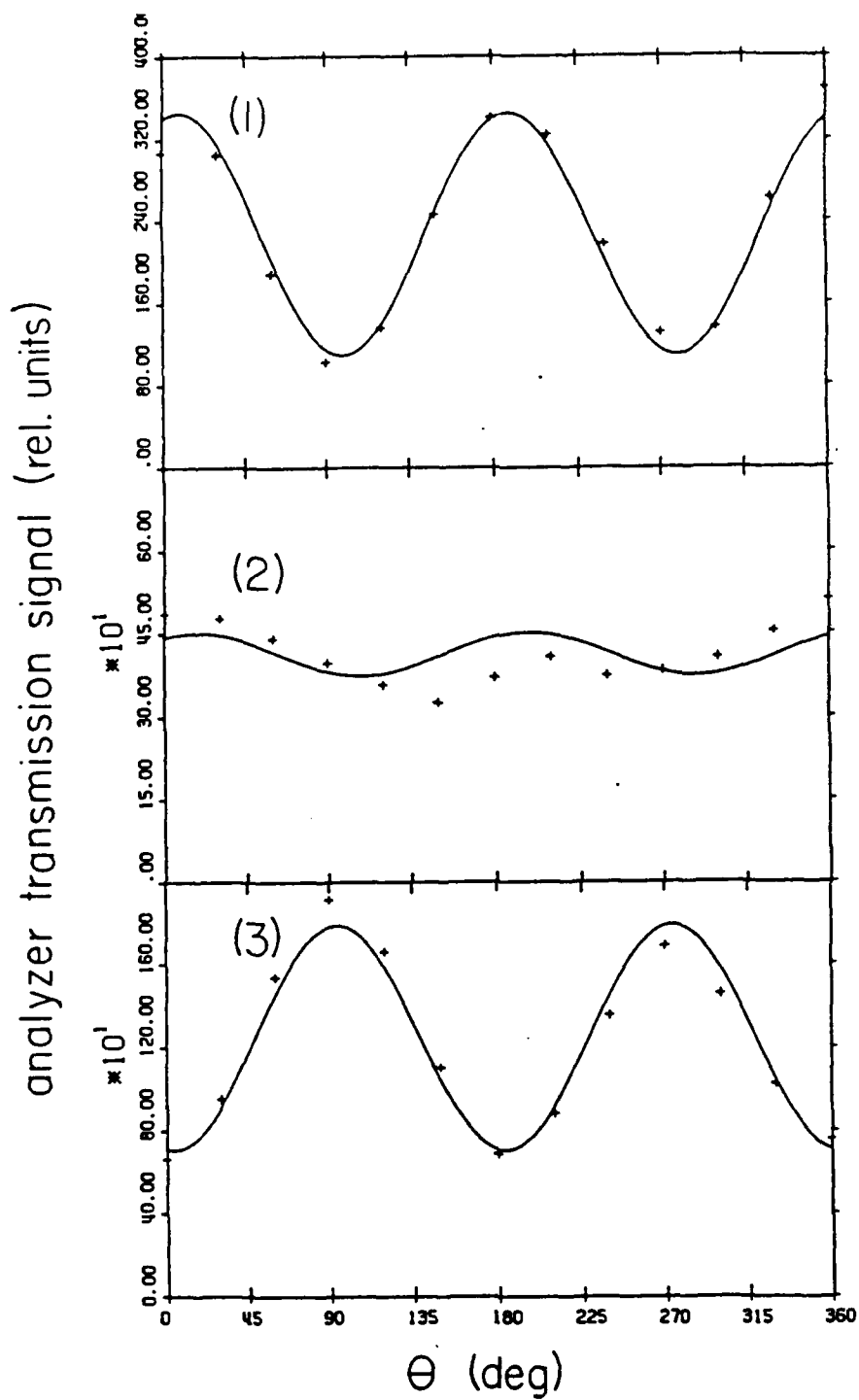


Figure 17. Analysis of SF ellipticity orientation versus laser detuning. (Each case shown corresponds to a detuning noted () in Figure 15.)

In particular, for large detunings such that $\chi/\Delta \leq 0.75$, the ratio of I_{\perp}/I_{\parallel} is in reasonable accord with the predictions in Reference 19 for Rayleigh plus collisional transfer to each of the m_J levels (Fig. 18); here the calculations of optical collision cross sections are given in turn by the Light and Szöke model as refined by Kleiber, et al., (Ref. 21).

There are still a number of experimental shortcomings of this work which are to be addressed presently: good accounting of the pump laser's spatial and temporal structure are needed to determine the strength of interaction χ , and optical trapping of resonance fluorescence must be rigorously assessed before effects of strong field collisional depolarization can be easily interpreted.

Of more subtle note is the observation that for small detuning where $\chi/\Delta \geq 1$, the ratio of I_{\perp}/I_{\parallel} becomes very sensitive to stimulated emission by the three- and four-photon scattering processes noted in Figure 6. Thus future goals of this work include performing these measurements with a single longitudinal mode (SLM) dye laser in order to determine χ more effectively, and reduce (pump laser) ASE to minimize externally induced stimulated emissions at ω_3 and ω_4 . Effects of optical trapping and radiative redistribution will be assessed more quantitatively by measuring the excited state m_J and velocity distributions directly with a probe CW-SLM diode laser.

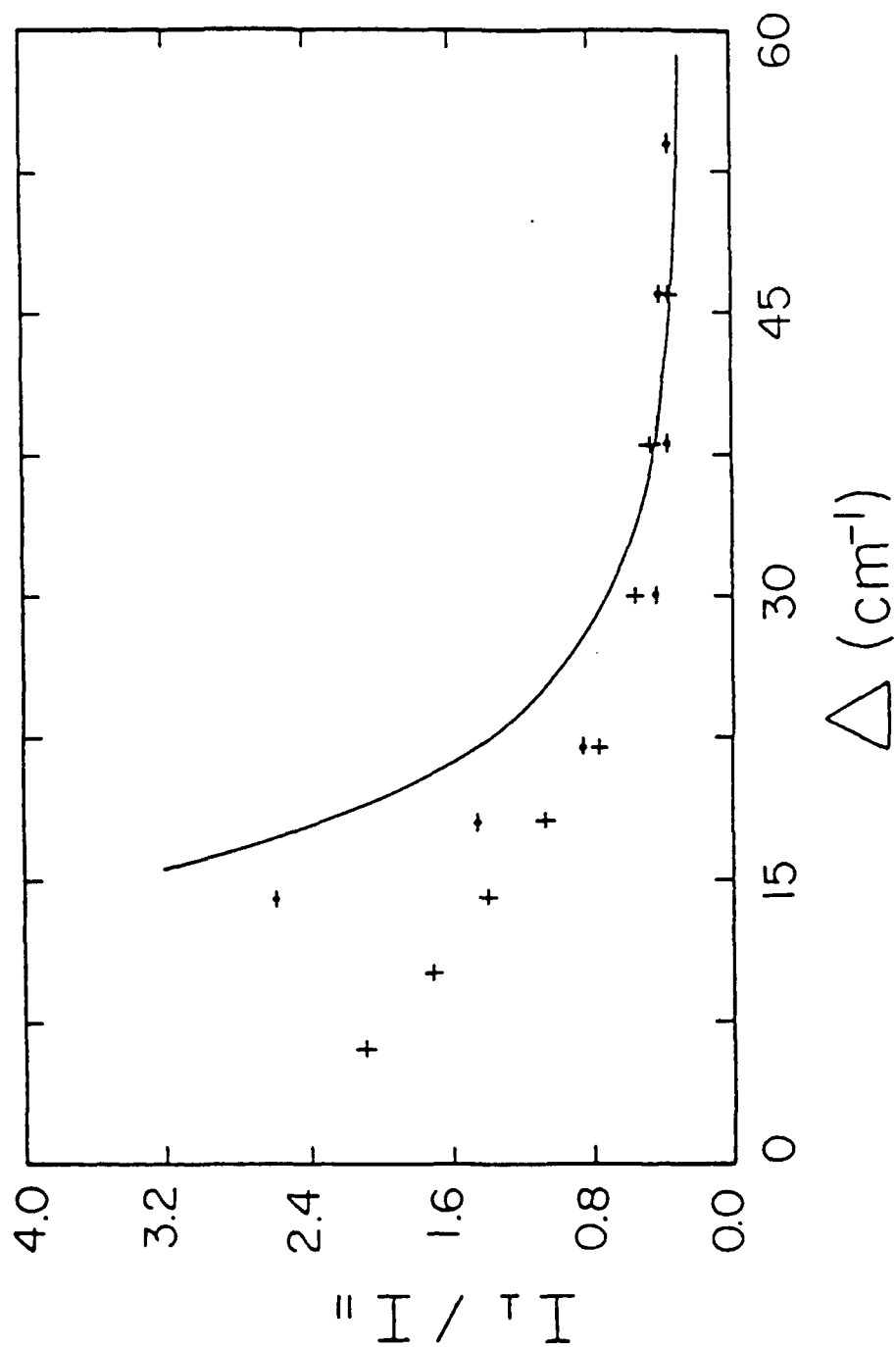


Figure 18. Ratio of linear polarization components versus laser detuning. (+ denotes cases of blue detunings while x denotes red detunings. The solid curve shows a rate equation calculation of the M_J distributions weighted by the Wigner 3-J coefficients for subsequent emission.)

4.4 HYPER-RAMAN SCATTERING AND CASCADE SF EMISSIONS IN Ca

Lasing action from a two-photon excited state to lower intermediate levels was suggested in Reference 22 and is now a well-known method of frequency down-conversion (usually to the IR) by so-called hyper-Raman scattering. There have also been several studies of SF cascade emission when high lying levels are populated by two-photon transitions, and the first optical SF emissions were observed by Cahuzac, et al., (Ref. 23) in a cascade sequence in Eu.

A considerable number of optical SF cascades which occur when $[Ca(4^1S_0)] > 3 \times 10^{14} \text{ cm}^{-3}$ and the pump irradiance exceeded $> 30 \text{ MW/cm}^2$ have also been observed. Several of these visible cascade emissions had reasonable pulse energies ($\sim 1\text{--}5 \text{ }\mu\text{J}$ per pulse) and could be readily observed by the naked eye without blocking the remaining pump pulse. Since these strong visible emissions were often several cascades below the initially excited Rydberg levels, it is inferred that the initial scattering from, and/or population transfer into, high lying states is occurring with reasonable quantum yields ($> 5\%$) of the pump photons.

In addition to off-resonant two-photon excitation, a new collision induced pathway was observed. There are many final state Rydberg levels which can be stimulated readily when the pump laser detuning $-\Delta$ is such that $2\hbar\omega_L$ matches the energy separation to even parity, $J = 0$ or 2 final states. These same states were readily excited also when the laser is detuned 2Δ as shown in Figure 19.

The more surprising result of this work is that several cascades that are induced by the two-photon process do not get induced by the two-step collisionally aided process. There is no ready explanation for the apparent disparity of different branching channels. The cascades which occurred when pumping the $Ca(5s5d^1D_2)$ level by both methods are listed in Table 1. Both

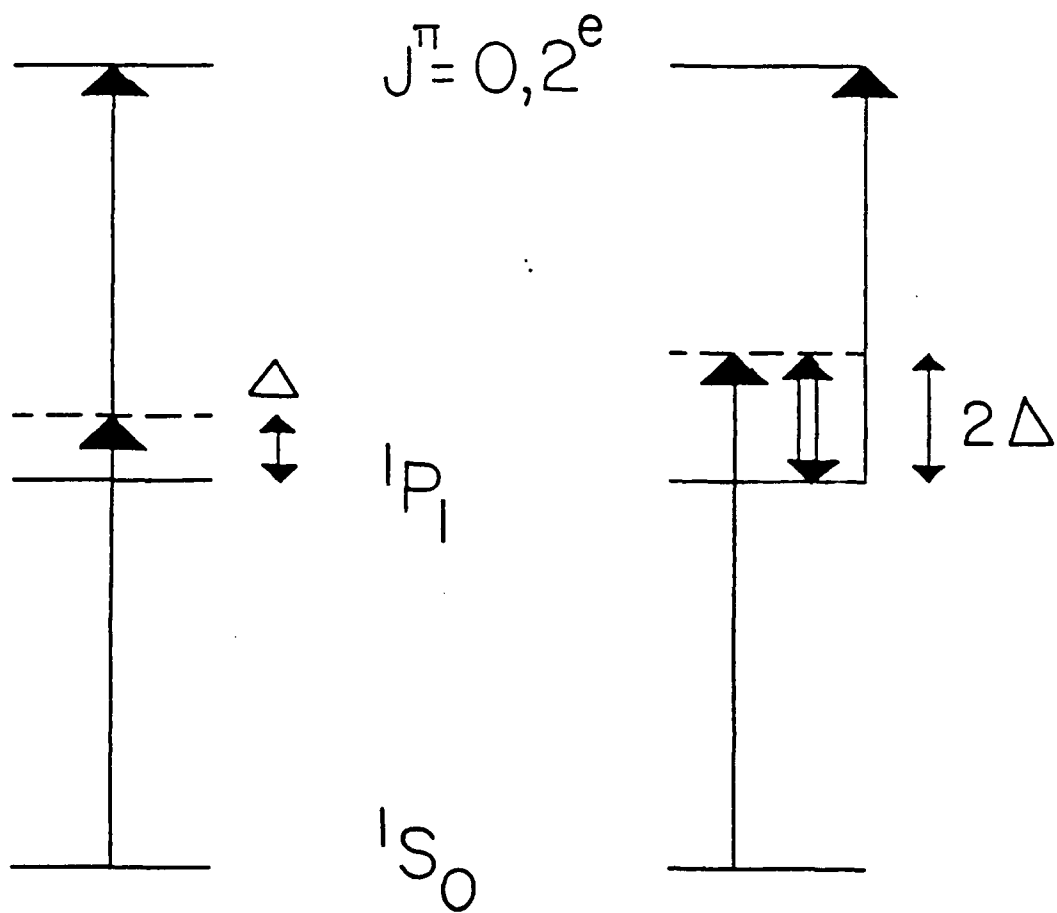


Figure 19. Two-photon and two-step collisionally aided excitation of Rydberg levels.

Table 1. The SF cascades which occur from pumping Ca ($5s5d\ ^1D_2$).

#	Transition	(Vacuum)	Δ	2Δ
1	$4s9d\ ^1D_2-4s5p\ ^1P_1$	9024.6 Å	-	+
2	$3d5s\ ^1D_2-3d4p\ ^1P_1$	2.8 μm	+	+
3	$4s9p\ ^1P_1-4s7s\ ^1S_0$	3.4 μm	+	+
4	$4s7f\ ^1F_3-3d4s\ ^1D_2$	3973.7 Å	+	-
5	$4s8d\ ^1D_2-3d4p\ ^1P_1$	3.3 μm	+	-
6	$4s9s\ ^3S_1-4s5p\ ^3P_J$	9810.1 Å	+	-
7	$4s8p\ ^1P_1-4s7s\ ^1S_0$	4.5 μm	+	+
8	$4s8p\ ^1P_1-3d4s\ ^1D_2$	4060 Å	+	-
9	$4s7d\ ^3D_J-4s6p\ ^1P_1$	2.16 μm	-	+
10	$4s7d\ ^1D_2-4s6p\ ^1P_1$	2.21 μm	+	-
11	$4s8s\ ^1S_0-4s4p\ ^1P_1$	4497.4 Å	-	+
12	$4s7p\ ^1P_1-4s7s\ ^1S_0$	8.7 μm	+	+
13	$4s7p\ ^1P_1-4s6s\ ^1S_0$	2.11 μm	+	+
14	$4s6d\ ^1D_2-4s6p\ ^1P_1$	3.0 μm	+	+
15	$4s6d\ ^1D_2-4s4p\ ^1P_1$	4686.9 Å	+	-
16	$4s5g\ ^1G_4-4s4f\ ^1F_3$	3.9 μm	+	+
17	$4s5f\ ^1F_3-4s5d\ ^1D_2$	5.3 μm	+	+
18	$4s7s\ ^1S_0-4s6p\ ^1P_1$	3.8 μm	+	+
19	$4s7s\ ^1S_0-4s4p\ ^1P_1$	4848.7 Å	+	+
20	$3d4p\ ^1P_1-4s6s\ ^1S_0$	3.1 μm	+	+
21	$3d4p\ ^1P_1-3d4s\ ^1D_2$	4528.2 Å	+	+
22	$4s5d\ ^1D_2-4s6p\ ^1P_1$	8.1 μm	+	+
23	$4s5d\ ^1D_2-4s4p\ ^1P_1$	5190.3 Å	+	-

Table 1. (Concluded.)

#	Transition	(Vacuum)	Δ	2Δ
24	$4s4f\ ^1F_3-4s4d\ ^1D_2$	$1.98\ \mu\text{m}$	+	+
25	$4s4f\ ^1F_3-3d4s\ ^1D_2$	$4879.5\ \text{\AA}$	+	-
26	$4s6p\ ^3P_J-3d4s\ ^3D_J$	$4510.7\ \text{\AA}$	+	-
27	$4s6p\ ^1P_1-4s4d\ ^1D_2$	$4380.7\ \text{\AA}$	+	+
28	$4s6p\ ^1P_1-3d4s\ ^1D_2$	$5043.0\ \text{\AA}$	+	+
29	$4p^2\ ^1S_0-4s4p\ ^1P_1$	$5514.5\ \text{\AA}$	+	-
30	$4s6s\ ^1S_0-4s5p\ ^1P_1$	$2.5\ \mu\text{m}$	+	+
31	$4s4d\ ^1D_2-4s4p\ ^1P_1$	$7328.2\ \text{\AA}$	+	-
32	$4s5p\ ^1P_1-4s5s\ ^1S_0$	$2.9\ \mu\text{m}$	+	+
33	$4s5p\ ^1P_1-3d4s\ ^1D_2$	$6719\ \text{\AA}$	+	-
34	$4s4p\ ^1P_1-3d4s\ ^1D_2$	$5.55\ \mu\text{m}$	+	+
35	$3d4s\ ^3D_3-4s4p\ ^3P_2$	$1.97\ \mu\text{m}$	+	+

sets of data were obtained under the same buffer pressure and pump irradiance. Presumably, collisional transfer and dephasing after the pump process should be the same, so it is inferred that some feature of the coherence of radiative excitation is being altered by the collisions during excitation.

An energy balance estimation has shown that some 10 percent or more of the pump photons can be transferred by the two-photon or two-step processes. It is uncertain whether any of the initial scattering processes from $\text{Ca}(5s5d\ ^1D_2)$ yielded tunable Raman scattering, although the tuning range for excitation was $\sim 1\text{-}3\ \text{cm}^{-1}$ wide. The longer-IR emissions that were likely supplying many of the cascades that fed the higher nearby P and F states could not be studied. However, two other two-photon transitions were studied ($4s10s\ ^1S_0$ and $5s3d\ ^3D_2$). These

transitions produced similar behavior as that noted here for the $5s5d\ ^1D_2$ case.

A second interesting result was the observation that the visible SF emissions were substantially foreshortened compared to the pump laser. These observed pulses were as short as the instrument limited bandwidth of the electronics (500 MHz \rightarrow 1.4 ns FWHM) although the feed-in IR cascades were considerably longer in duration (see Figs. 20a and b for a comparison). There is no explanation why this might be so since one would expect regenerative emissions to occur if the feed-in cascades last much longer.

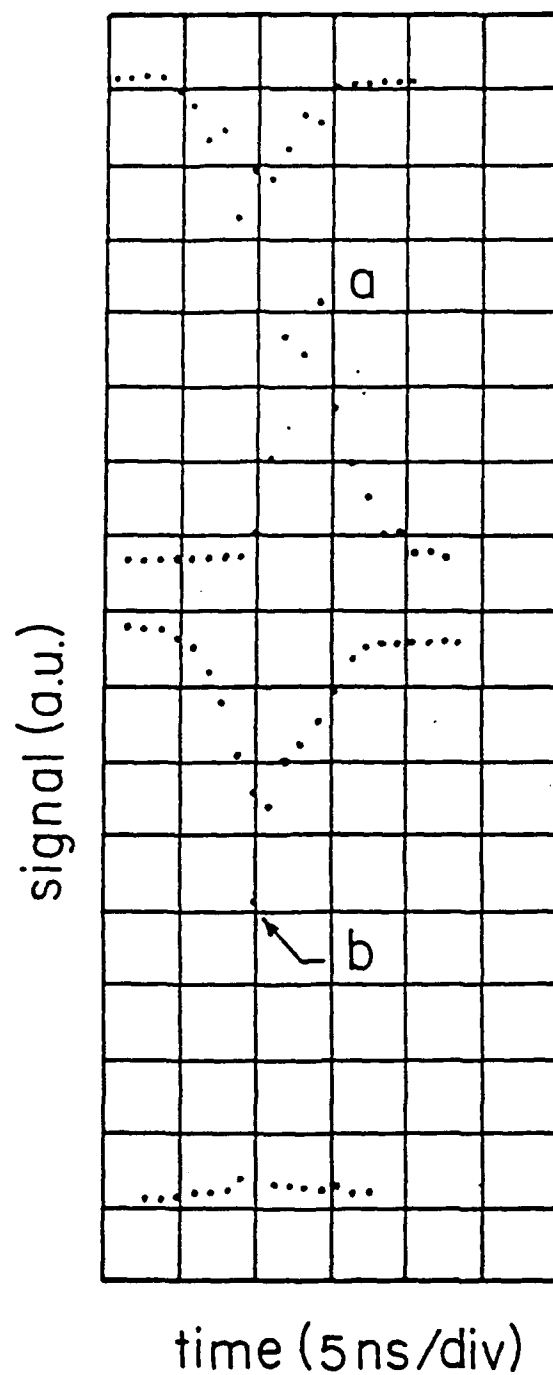


Figure 20. Comparison of IR SF cascade and its successive optical SF emission. (A shows the SF which occurs on the $4s7s\ ^1S_0 - 4s6p\ ^1P_1$ transition at $3.8\ \mu\text{m}$, and B shows the resultant SF cascade on the $4s6p\ ^1P_1 - 3d4s\ ^1D_2$ transition at 5043 angstroms.)

5.0 CONCLUSIONS

It appears unlikely that efficient SRS can be initiated spontaneously in Raman amplifiers whenever the oscillator strength for the pump transition is substantially larger than the Stokes transition. A variety of three- and four-photon scattering processes involving the Rabi-split sidebands of the pump transition will be more efficient in transferring population to the intermediate state as has been observed. These processes lead to SF at the fixed wavelength for the down converting transition, even in the absence of significant collisional transfer.

The observed SF emissions are very interesting in their own right. The emissions by $\text{Ca}(4^1\text{P}_1-3^1\text{D}_2)$ or its analog in Sr could be used as an experimental test bench to study SF gain in plasma based X-ray laser systems. Evidence suggests that some highly ionized X-ray lasers exhibit the type of multiple pulse ringing seen (Ref. 24). These plasma-based systems are operationally analogous to the $\text{Ca}(4^1\text{P}_1-3^1\text{D}_2)$ SF mechanism in that they release their optically trapped excited state populations on less favored transitions. Issues of quantum yield and temporal pulse shaping could be explored more readily in the Group IIA metals. In a related manner principal transitions for Ca and Sr are potentially suitable candidates to use in an electrical discharge laser analogous to the Cu-vapor laser. If one operated this discharge at low buffer pressures, the mid-IR emissions at 5.5 and 6.5 μm could perhaps be efficiently generated. Adding ~5-10 Torr of Ar in the Ca system and 0.5 Torr in Sr could allow strong fixed emissions by their respective lowest $3\text{D}_3-3\text{P}_2$ transitions near 2 μm for Ca and 2.9 μm for Sr.

REFERENCES

1. Dicke, R. H., Phys. Rev. 93, p. 99 (1954).
2. Bonifacio, R. and Lugiato, L. A., Phys. Rev. A 11, p. 1507 (1975).
3. Schuurmans, M. F. H., Vrehen, Q. H. F., Polder, D., and Gibbs, H. M., Adv. Atomic and Mol. Physics, ed. by D. Bates and B. Bederson, Academic Press (1981).
4. Szöke, A., Opt. Lett. 2, p. 36 (1978).
5. Light, J. and Szöke, A., Phys. Rev. A 18, p. 1363 (1978).
6. Burnett, K., Phys. Repts. 118, p. 339 (1985).
7. Wenzel, R. G., Telle, J. M., and Carlsten, J. L., J. Opt. Soc. Am. A3, p. 838 (1986).
8. Breckenridge, W. H. and Merrow, C. N., J. Chem. Phys. 88, P. 2320 (1988).
9. Kelly, J. F., Harris, M., Cooper, J., and Gallagher, A., Sixteenth International Conference on Physics of Electronic and Atomic Collisions, ed. by A. Dalgarno, R. S. Freund, M. S. Lubell and T. B. Lucatorto, p. 87 (1989).
10. Raymer, M. G. and Carlsten, J. L., Phys. Rev. Lett. 39, P. 1326 (1977).
11. Herman, B. J., Eberly, J. H., and Raymer, M. G., Phys. Rev. A 39, p. 3447 (1989).
12. Kinoshita, S. and Kushida, T., Phys. Rev. A 42, p. 2751 (1990).
13. Schuurmans, M. F. H., Opt. Commun. 34, p. 185 (1980).
14. Arecchi, F. T. and Courtens, E., Phys. Rev. A 2, p. 1730 (1970).
15. Gross, M. and Haroche, S., Phys. Repts. 93, p. 301 (1982).
16. Maki, J. J., Malcuit, M. S., Raymer, M. G., Boyd, R. W., and Drummond, P. D., Phys. Rev. A 40, p. 5135 (1989).
17. Malcuit, M. S., Maki, J. J., Simkin, D. J., and Boyd, R. W., Phys. Rev. Lett. 59, p. 1189 (1987).
18. Wright, J. J. and Balling, L. C., J. Chem. Phys. 73, p. 1617 (1980).

REFERENCES (Concluded)

19. Courtens, E. and Szöke, A., Phys. Rev. A15, p. 1588 (1977).
20. Carlsten, J. L., Szöke, A., and Raymer, M. G., Phys. Rev. A15, p. 1029 (1977).
21. Kleiber, P. D., Cooper, J., Burnett, K., Kunasz, C. V., and Raymer, M. G., Phys. Rev. A27, p. 291 (1983).
22. Grischkowsky, D., Loy, M. M. T., and Liao, P. F., Phys. Rev. A12, p. 2514 (1975).
23. Cahuzac, Ph., Sontag, H., and Toschek, P. E., Opt. Commun. 31, p. 37 (1979).
24. Kapteyn, H. C. and Falcone, R. W., Phys. Rev. A37, p. 2033 (1988).